# Gemcitabine, vinorelbine and cyclooxygenase inhibitors in the treatment of glioblastoma. Ultrastructural analyses in C6 glioma *in vitro*

İlhan Elmaci[a], Ayhan Bilir[b], Aysel Ozpinar[c], Meric A. Altinoz[c,d,*]

[a] *Department of Neurosurgery, Acibadem Hospital, Istanbul, Turkey*
[b] *Department of Histology and Embryology, Aydin University, Istanbul, Turkey*
[c] *Department of Medical Biochemistry, Acibadem University, Istanbul, Turkey*
[d] *Department of Psychiatry, Maastricht University, Holland*

ABSTRACT

*Objectives:* To define ultrastructural features accompanying to antitumor effects of gemcitabine, vinorelbine and cyclooxygenase inhibitors in C6 glioma cells in vitro. Vinorelbine is a semisynthetic vinca alkaloid and recent studies showed its antitumor activity in pediatric optic and pontine gliomas. Vinorelbine infusion induces a severe tumor site-pain in systemic cancers, but it is unknown whether algesia and inflammation contribute to its antitumor effects. Gemcitabine is a nucleoside-chemotherapeutic which was recently shown to act as a radio-sensitizer in high-grade glioma. Some studies showed synergism of anti-inflammatory cyclooxygenase-inhibitors with microtubule inhibitors and gemcitabine. DMSO is a solvent and blocks both cylooxygenase and ribonu-cleotide reductase, another target of gemcitabine. Rofecoxib is withdrawn from the market, yet we used it for investigational purposes, since it blocks cylooxygenase-2 1000-times more potently than cylooxygenase -1 and is also a selective inhibitor of crinophagy.
*Methods:* Plating efficacy, 3D-spheroid S-phase analysis with BrdU labelling and transmission electron micro-scopical analyses were performed.
*Results:* Vinorelbine induced frequent mitotic slippage/apoptosis and autophagy. Despite both DMSO and ro-fecoxib induced autophagy alone and in synergy, they reduced mitotic catastrophe and autophagy triggered by vinorelbine, which was also reflected by reduced inhibition of spheroid S-phase. Gemcitabine induced karyolysis and margination of coarse chromatin towards the nuclear membrane, abundant autophagy, gutta adipis for-mation and decrease in mitochondria, which were enhanced by DMSO and rofecoxib.
*Conclusions:* Detailed ultrastructural analysis of the effects of chemotherapeutic drugs may provide a broader insight about their actions and pave to develop better strategies in treatment of glioblastoma.

## 1. Introduction

In glioblastoma, maximum surgical resection, radiotherapy, and adjuvant temozolomide is the golden standard of care, yet it could only provide a median survival around 15 months (Altinoz et al., 2016). This is a an untolerable rate of mortality; hence, development of further chemotherapy protocols is a priority for the physicians and basic sci-entists. Since the beginning of the 21th century, huge amounts of new data emerge about cancer's metabolomic responses against therapeutic modalities thanks to the techniques such as microarrays, next-genera-tion sequencing methods and improved mass spectrometric analyses. Nonetheless, the obtained data is immense and even the data of a single paper need to be explained by many other papers. We believe that the detailed fine structural analysis of cancer cell responses against various

treatments may provide a broader view to understand the action me-chanisms of antineoplastic drugs and complement molecular data. In this study, we focused on the effects of vinorelbine, gemcitabine and cyclooxygenase inhibitors on the fine structure of C6 glioma cells due to the facts that: (i) vinorelbine and gemcitabine were recently shown to have activity in highly fatal glial tumors; (ii) cyclooxygenase inhibitors were shown to synergy with temozolomide in glioblastoma cells; (iii) lack of studies which analyzed fine structural responses of cancer cells to vinorelbine, gemcitabine and cyclooxygenase inhibitors especially in glial tumors. We have previously published a short description of the ultrastructural changes induced by the mentioned agents (Tuna et al., 2009). "Materials and Methods" described below were mostly described in our previous article; and 3 of the 52 different electron microscopical pictures which we submit with our current article (Fig. 2B, Fig. 10C,

Fig. 13D) are the same of our previous publication (Fig. 4A, C and D of Reference-2), which we also mentioned in Figure Legends. Our intention in this study is to intensely focus on the effects of chemotherapeutic agents on the fine structure of glioma cells. Hence, cell kinetic data were given to strengthen our proposals in regard to action mechanisms of chemotherapy agents and cyclooxygenase inhibitors.

## 2. Materials and methods

As mentioned above, "Materials and Methods" were mostly described in our previous article.

### 2.1. Monolayer culture, plating efficacy and drug treatments

C6 cells established from the American Type Culture Collection (ATCC) were maintained in Dulbecco's modified Eagle's Medium (DMEM, containing 100 U/ml penicillin and 100 µg/ml streptomycin) (Biological Industries, Haemek, Israel) supplemented with 10% heat inactivated foetal bovine serum (FBS) (Biological Industries, Haemek, Israel). The flasks were kept in an incubator with a humidified atmosphere of 5% $CO_2$ at 37 °C. Cells were transferred using $Ca^{2+}$ and $Mg^{2+}$ free Hanks' basic salt solution and 0.25% trypsin- and ethylendiamine tetraacetic acid (EDTA) (Biological Industries, Haemek, Israel). We used early passages (4–7 t h) of C6 cells after obtaining the cell line. Vinorelbine tartrate (Navelbine®, Pierre Fabre Medicament), Gemcitabine (Gemzar®, Lilly), rofecoxib (Merck Sharp & Dohme) and DMSO (D2650, Sigma) were dissolved in bidistilled water and added into cell culture in equal volumes. To obtain the dose-response curves of vinorelbine tartrate, gemcitabine and rofecoxib, increasing concentrations of 1, 10 and 100 µg/ml were applied for each drugs, respectively; and cells were counted on a Thoma chamber following 24, 48, 72 and 96 h after treatment. Vinorelbine tartrate concentrations of 1, 10 and 100 µg/ml corresponded to 0.927, 9.27 and 92.7 µM, respectively. Gemcitabine concentrations of 1, 10 and 100 µg/ml corresponded to 3.78, 37.8 and 378 µM, respectively; and rofecoxib concentrations of 1, 10 and 100 µg/ml corresponded to 3.18, 31.8 and 318 µM, respectively. Except the dose-response experiments, all chemotherapy agents including gemcitabine, vinorelbine and rofecoxib were applied at a dosage of 10 µg/ml to the cell cultures. DMSO concentration was constant for all experiments (cell counts, spheroid BrdU labeling, electron microscopy) which was 20 µl/ml.

### 2.2. D-spheroid culture

Spheroids were obtained by inoculating $10^6$ cells into 10 ml of 10% DMEM-FBS in petri dishes on a thin layer of agar (10 ml of a 0.75% (w/v) solution of agar in DMEM-FBS 10%). Spheroids (approximately 2000–4000 cells per spheroid) were harvested by gentle transfer of individual spheroids into the wells of a 24-well culture plate using a micropipette.

Multicellular Tumour Spheroids (MTS) were then individually placed into the wells of a 24-well culture plate containing 1 ml of DMEM-FBS 10% on a layer of 1 ml of 0.75% (w/v) agar in the same medium. Every 7 days, 0.5 ml of DMEM medium was gently removed from each well and the wells were then filled with the some amount of fresh medium.

### 2.3. Bromodeoxyuridine-labelling index (BrdU-LI) in spheroid culture

BrdU (5-bromo-2-deoxyuridine (2 µM, 1:200 dilution) was added to the spheroids medium with subsequent incubation for 1 h. Thereafter, spheroids were gently removed from the surface of the solidified agar and transferred into phosphate buffer saline (PBS, pH 7.4). Spheroids were fixed in 4% paraformaldehyde (Sigma Chemical Co., St. Louis, Missouri, USA) in PBS for 24 h at 4 °C and then again transferred into pure phosphate-buffered saline (PBS). Following fixation, the spheroids were dehydrated through graded ethanol series, cleared in xylene,

embedded in paraffin and 5 µm coronal sections were cut on microtome (Leica MR 2145, Heerbrugg, Switzerland). Sections were dewaxed in xylene for 30 min. After soaking in decreasing series of ethanol, sections were washed with distilled water and PBS for 10 min and then treated with 2% trypsin in 50 mM Tris buffer (pH 7.5) at 37 °C for 15 min and washed with PBS. Sections were incubated in a solution of 3% $H_2O_2$ for 15 min, then washed with PBS and incubated with primary mouse anti-BrdU antibody (1:250 dilution, LabVision, UK). Next, the sections were incubated with biotinylated IgG followed by streptavidin- peroxidase conjugate (LabVision, UK). The sections were then washed and incubated with the AEC chromogen substrate system and counterstained with Mayer's haematoxylin. The immunostained slides were observed under light microscopy at magnifications of x 40. BrdU-labelled cells were evaluated by the same person. BrdU-positive cell were defined by observing dark red AEC nuclear staining. Unlabelled nuclei with only blue haematoxylin staining and pale brownish nuclei were considered to be negative. Ten adjacent sections and at last 3000 cells were evaluated for each group.

### 2.4. Transmission electron microscopical analysis

The harvested spheroids were fixed with 2% glutaraldehyde in 0.1 mol/L sodium cacodylate (pH 7.4) for 1 h at 4 °C. Samples were then washed twice for 10 min with sodium cacodylate with a pH value of 7.4. They were then fixed with 2% osmium tetraoxide in 0.1 M sodium cacodylate for 1 h at room temperature. Samples were then washed 3 times for 5 min each with the same buffer. Cells were exposed to 1% uranyl acetate for 1 h and washed again 3 times for 10 min each with the same buffer. Samples were dehydrated via graded ethanol series. After embedding in Epon-812 (SPI Chem., Pensylvania, USA), samples were sectioned to a thicknesses of 700–800 A° on a Richert Ultramicrotom (OMS, Austria). Sections were post-stained with 5% uranyl acetate for 30 min, followed by Reynolds lead citrate incubation. Samples were then examined with a Jeol 1011 transmission electron microscope.

### 2.5. Statistical analysis

All data were expressed as the mean ± SEM. Statistical analysis was performed by the 2-tailed Student *t*-test The accepted level of significance was set at $P > 0.05$.

## 3. Results

### 3.1. Fine structural findings

#### 3.1.1. Control group
The morphology of C6 glioblastoma cells in the control group is shown in Fig. 1 and Fig. 2. Abundant filopodia and gap junctional cell-to-cell adhesions were observed. The cell nuclei had evenly dispersed heterochromatin sometimes with well developed nucleoli with discernible granulary and fibrillary components (Fig. 1a). Peculiarly, some cells exhibited nuclei which only contain euchromatin in absence of any signs of cell death likely indicating prominent gene transcription (Fig. 1b). The cytoplasm contained abundant and easily discernible rough ER (Fig. 1b). Abundant mitochondria were witnessed in some cells which seemed to be more in cells with more filopodia (Fig. 1c, Fig. 2a, 2b). Normal metaphase figures with proper chromosal alignement and polar microtubules were seen in which cellular cytoplasm contained abundant mitochondria mostly in tubular form (Fig. 2c, 2d). In a minority of cells, few autophagosomes and autophagolysosomes were seen. In few cells, glycogen accumulations can be discerned.

#### 3.1.2. DMSO
The morphology of C6 glioblastoma cells in the DMSO group is shown in Fig. 3. Filopodia were lost and cell became more rounded with
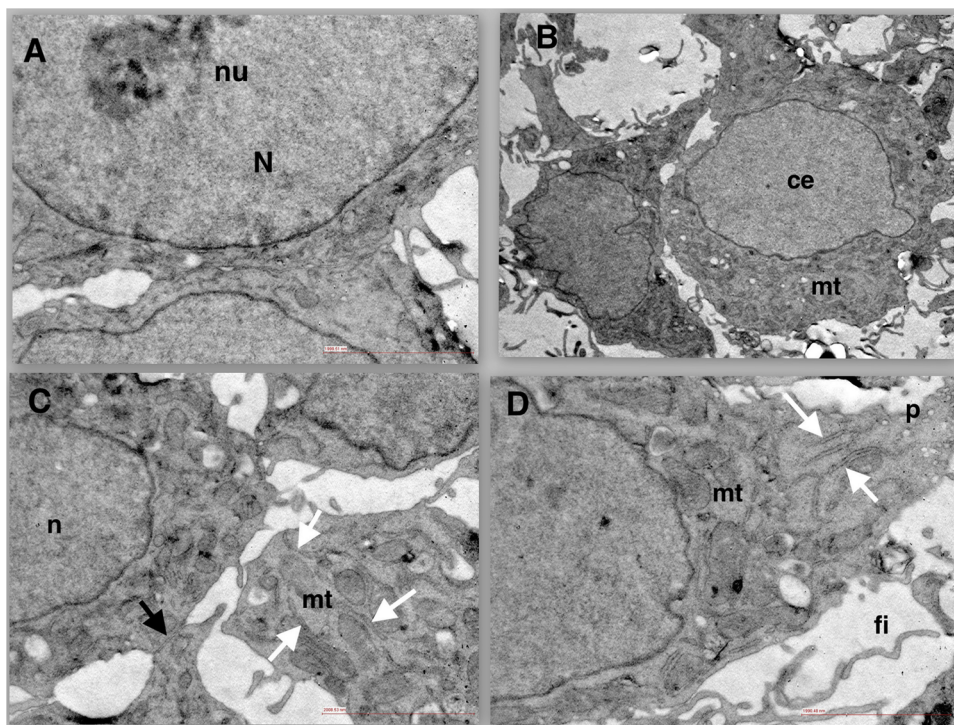
**Fig. 1.** Morphology of C6 glioblastoma cells in the control group. a) The cell nuclei (n) had evenly dispersed heterochromatin sometimes including well developed nucleoli (nu) with discernible granulary and fibrillary components (x20000 m). b) Some cells exhibited nuclei which only contain complete euchromatin (ce) in absence of any signs of cell death. Mitochondria (mt) were healthy with no darkening/condensation (x7500 m). c) Gap junctional cell-to-cell adhesions were observed (black arrow). Abundant healthy mitochondria (mt) in tubular form were witnessed (x20000 m). d) Mitochondria juxtaposing the cell nucleus and easily discernible membranes of the endoplasmic reticulum (white arrows) were seen. Pinocytosis vesicles (p) were witnessed on the tip of the cytoplasm (x20000 m). m: magnification.

slight enhancement of cells with Type-1 apoptotic morphology. Mitochondrial numbers decreased and their morphology shifted more to spherical forms. Autophagosomes and autophagolysosomes increased and their contents contrasted similar to the cytoplasm. Desmosomal junctions developed. Occasional formations of gutta adipis (lipid droplets) were seen.

### 3.1.3. Rofecoxib

The morphology of C6 glioblastoma cells in the rofecoxib group is shown in Fig. 4 and Fig. 5. Filopodia were lost. Most nuclei lost their smooth oval contour and indentations became more frequent. In some cell nuclei, nucleoli became larger and more electron dense and dissociation of fibrillary and granular components were also noticed. Interestingly, some nuclei contained meiotic synaptonemal complex, which will be explained in discussion. Occasional pyknotic nuclei were seen in the absence of cytoplasmic blebbing. Mitochondrial numbers decreased and crista damage and swelling were witnessed in some mitochondria. Autophagosome and lysosome fusions and enhanced autophagolysosomes can be discerned in some cells. Lysosomal myelinosis suggestive of phospholipid accumulation and autophagic process
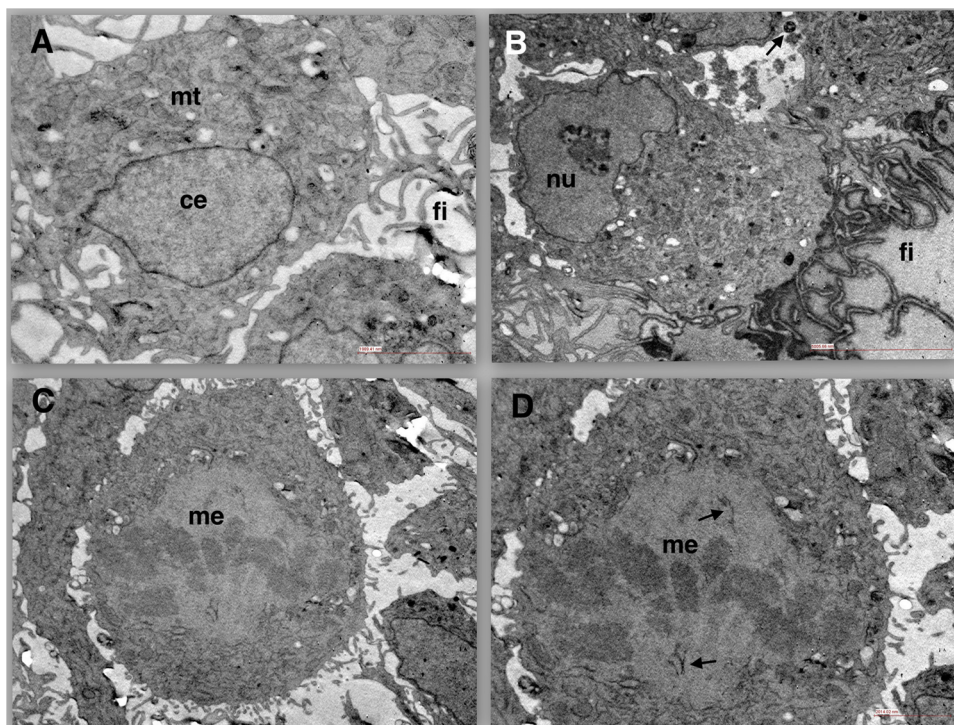


**Fig. 2.** Morphology of C6 glioblastoma cells in the control group. a) Note the complete euchromatin (ce), healthy mitochondria (mt) and abundant filopodia (fi) (x15000 m). b) Mitochondria and cytoplasmic organelle content seemed to be more abundant in cells with higher numbers of filopodia (fi). Nucleolar (nu) fibrillary and granular components can be differentiated in some cells (x7500 m). c) Normal metaphase (me) figures were seen in which cellular cytoplasm contained abundant mitochondria mostly in tubular form (x7500 m). d) Microtubules originating from spindle poles were discernible (thin black arrows) (x10000 m). m: magnification – Figure 2b was taken from the publication of Tuna et al. (2009) with permission (corresponding to the Figure 4a in the aforementioned manuscript).
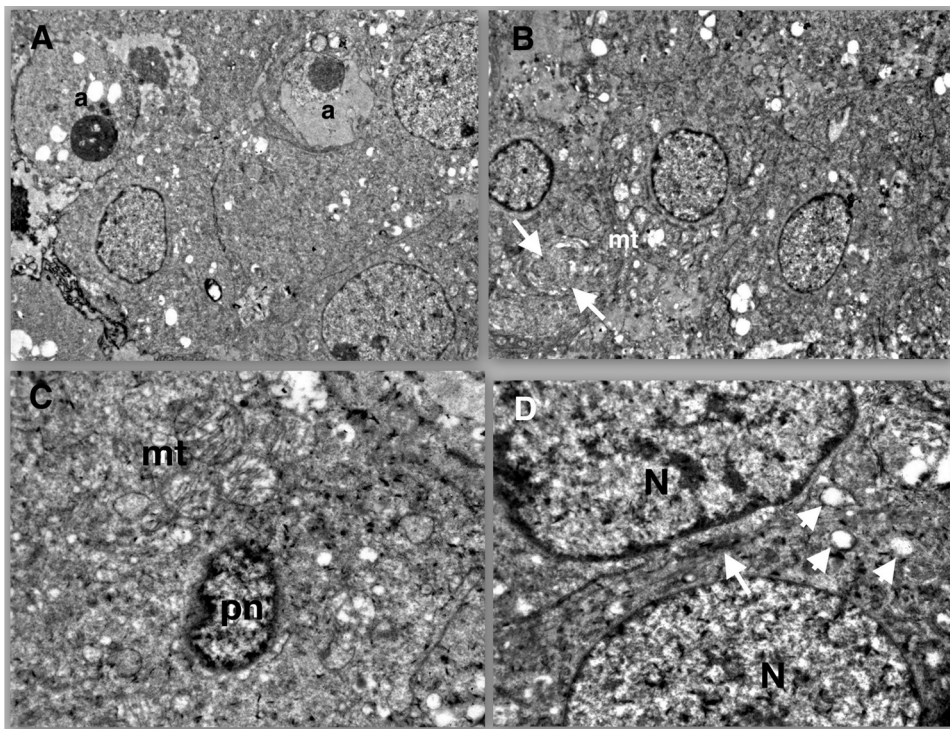
Fig. 3. Morphology of C6 glioblastoma cells in the DMSO-treated group. a) Filopodia were lost and cell became more rounded with slight enhancement of cells with apoptotic morphology (a). Some apoptotic cells were engulfed by neighbouring cells (x5000 m). b) Damage to mitochondrial cristae (mt) and endoplasmic reticulum whorls (white arrows) were witnessed. Occasional formations of gutta adipis (lipid droplets) were seen (x5000 m). c) A cluster of mitochondria juxtaposing a pycnotic cell nucleus (pn) (x12000 m). d) Autophagosomes and autophagolysosomes increased and their contents contrasted similar to the cytoplasm. Desmosomal junctions (white arrow) developed. Mitochondria lost their cristae (white arrowheads) (x12000 m). m: magnification.

were also observed. Occasional enwidening of ER cisternae was noticed.

### 3.1.4. Rofecoxib + DMSO

The morphology of C6 glioblastoma cells in the rofecoxib + DMSO group is shown in Fig. 6. Mitotic catastrophe, karyorrhexis/nuclear fragmentation and micronuclei formation were observed. Increased numbers of mitochondria with condensed matrix were seen. Microtubule aggregates were discernible in some cells.

### 3.1.5. Gemcitabine

The morphology of C6 glioblastoma cells in the gemcitabine group is shown in Fig. 7. Filopodia were lost. Karyolysis of the central heterochromatin and margination of electron-dense coarse chromatin towards the nuclear membrane was seen. Abundant autophagy and gutta adipis (lipid droplet) formation prevailed. Mitochondria were either lost and/or shrunken with more electron-dense matrix impairing their distinguishment from cytoplasm. In some cells, ER whorls surrounded pyknotic nuclei.
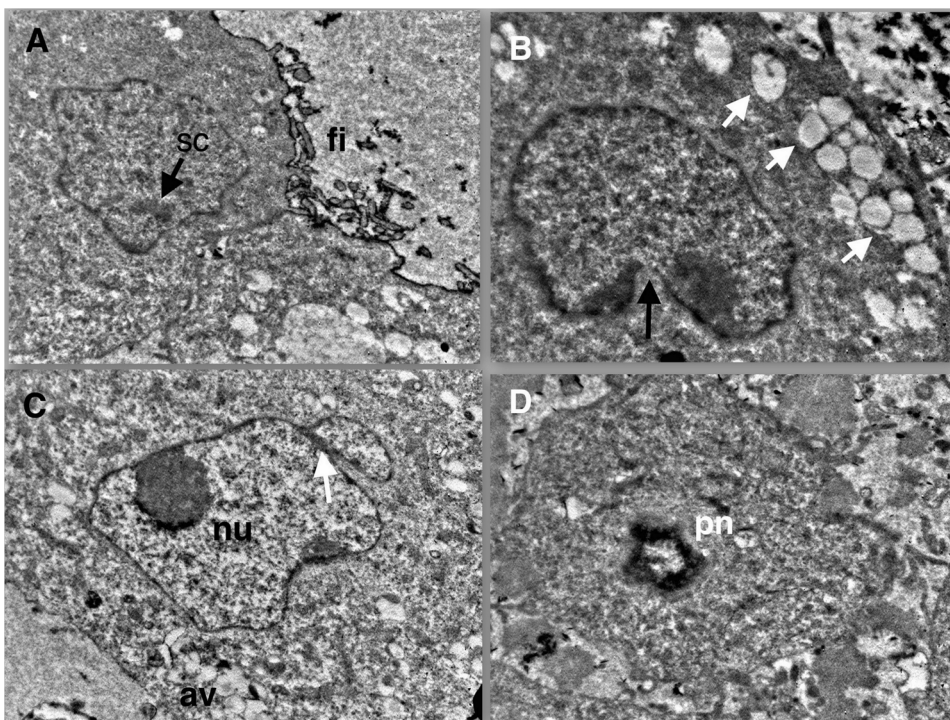


Fig. 4. Morphology of C6 glioblastoma cells in the rofecoxib-treated group. In general, filopodia were lost and most nuclei lost their smooth oval contour and indentations became more frequent. a) Fragmented and shortened filopodia (fi) on the cell surface and a synaptonemal complex (sc) in the nucleus (x10000 m). b) Darker and shorter mitochondria juxtaposing an indented cell nucleus (black arrow) were observed. Autophagosomes existed in in the cell periphery (white arrows) (x12000 m). c) A round enlarged nucleolus with dissociation of fibrillary and granular components (nu) and nuclear indentation (white arrow) (x12000 m). d) Occasional pyknotic nuclei (pn) were seen in the absence of cytoplasmic blebbing (x12000 m). m: magnification.
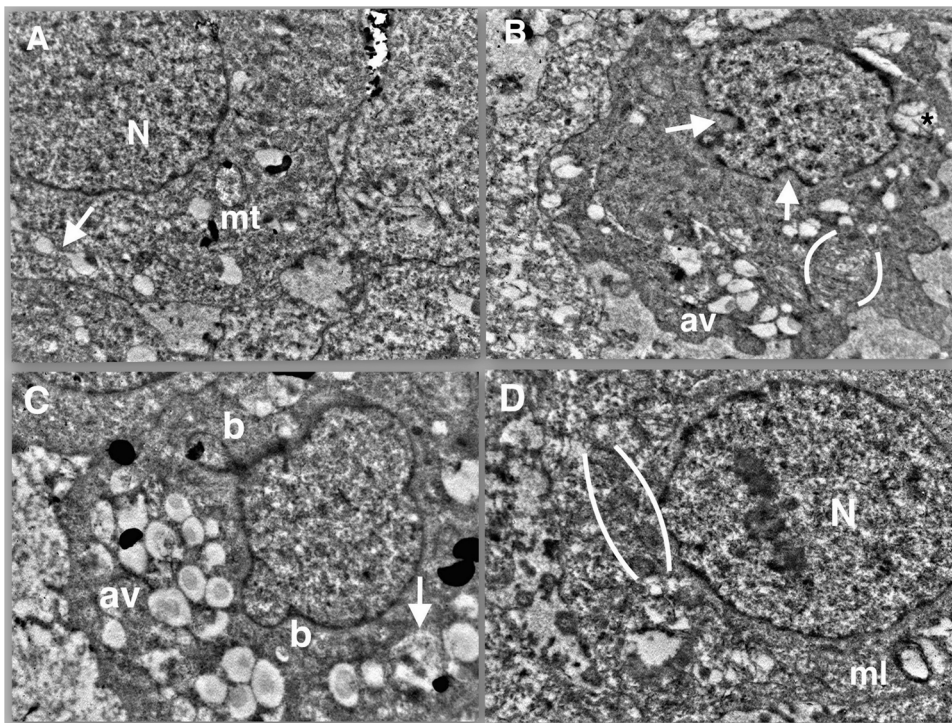
**Fig. 5.** Morphology of C6 glioblastoma cells in the rofecoxib-treated group. a) A damaged mitochondrion with fragmented cristae (mt) juxtaposing cell nucleus. Lysosome-autophagosome fusion in the cell periphery (white arrow) (x10000 m). b) Autophagosomes and autophagolysosomes in the cell periphery. Curved lines surrounds whorled and enlarged cisternae of the endoplasmic reticulum. Nuclear indentations (white arrows) and autophagic vacuoles (av) are discernible (x10000 m). c) Abundant autophagic vacuoles (av) in the cytoplasm. Blebbing (b) of the nuclear membranes and autophagolysosomes (white arrow) were discernible (x12000 m). d) Curved lines surround shrunken dark mitochondria beneath some larger mitochondria with crista damage. A myelinated lysosome (ml) is seen beneath the nucleus at the right lower side of the picture (x12000 m). m: magnification.

### 3.1.6. Gemcitabine + DMSO

The morphology of C6 glioblastoma cells in the gemcitabine + DMSO group is shown in Fig. 8. Filopodia were lost. Endosomes with irregular electron luscent material prevailed. Autophagolysosomes were also abundant and gutta adipis formations juxtaposed cell membranes. Mitochondria were either lost and/or shrunken with more electron-dense matrix impairing their distinguishment from cytoplasm. Cisternal enlargement of ER membranes and formations of stacks were seen. In some cells, ER membranes formed whorls, which did not surround other organelles rather collapsed within themselves.

Interestingly, meiotic synaptonemal complexes were witnessed in some nuclei.

### 3.1.7. Gemcitabine + Rofecoxib

The morphology of C6 glioblastoma cells in the gemcitabine + rofecoxib group is shown in Figs. 9 and Fig. 10. Filopodia were lost. Autophagolysosomes enhanced and coalesced into clusters which occasionally filled almost the whole cytoplasm. Gutta adipis formations enhanced further. Pyknotic nuclei became more frequent.
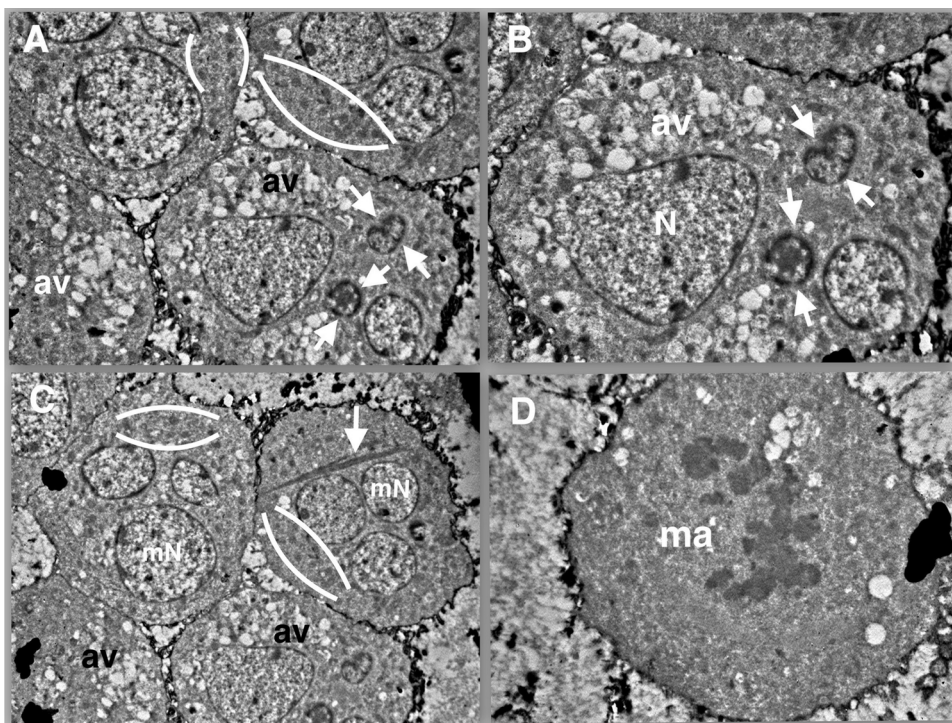


**Fig. 6.** Morphology of C6 glioblastoma cells in the DMSO + rofecoxib-treated group. Note the rounding of cells and nuclear fragmentation as a general feature. a) Nuclear fragmentation, condensed mitochondria (between white curved lines) surrounding cell nucleus at the upper right side of the picture (x5000 m). b) A higher magnification of the same area. A large cell containing abundant autophagic vacuoles (av) seemed to engulf neighbouring apoptotic cells. Apoptotic nuclei are engulfed by neighbouring cells (white arrows) (x7500 m). c) Nuclear fragmentation/micronuclei formation, condensed dark mitochondria (between curved white lines) and microtubule aggregates (white arrow) were witnessed (x4000 m). d) A cell undergoing mitotic apoptosis (ma) with lipid droplets / gutta adipis formations (x7500 m). m: magnification.
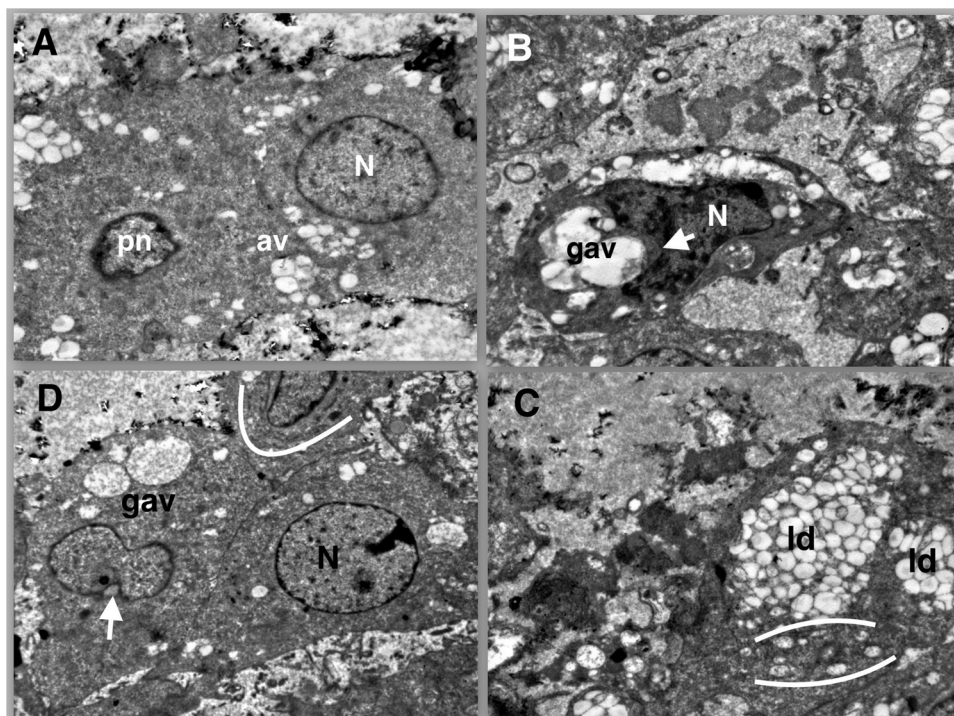
**Fig. 7.** Morphology of C6 glioblastoma cells in the gemcitabine-treated group. Filopodia were lost. a) Shrunken dark mitochondria juxtapose a dark nucleus. Autophagic vacuoles (av) and lipid droplets exist in the cell periphery of a relatively healthy and pycnotic (pn) nucleus (x6000 m). b) A glioma cell with dark cytoplasm. A nucleus with indentation and condensed coarse chromatin (white arrow) surrounds giant autophagic vacuoles (gav) (x7500 m). c) Cytoplasm is almost full with lipid droplets and autophagic vacuoles. Mitochondria with crista damage exist near the lipid droplet cluster (between white curves) (x7500 m). d) ER whorls surround a pyknotic nucleus (white surrounding curve). Giant autophagic vacuoles (gav) in the cell periphery (x5000 m). m: magnification.

### 3.1.8. Vinorelbine

The morphology of C6 glioblastoma cells in the vinorelbine group is shown in Figs. 11 and 12 . Strong and widespread autophagy prevailed with discernible endosomal / autophagosomal fusions. Chromatin precipitation into clumps, karyolysis and karyorrhexis/nuclear segregations were frequent. Frequent morphological signs of mitotic apoptosis/catastrophe were noticed, which simultaneously exhibited drastic autophagy. Prominent enlargement of ER cisternae were observed.

### 3.1.9. Vinorelbine + Rofecoxib

The morphology of C6 glioblastoma cells in the vinorelbine + rofecoxib group is shown in Fig. 13. Filopodia were lost yet nuclear contours became similar to controls and indentations were seen less frequently. Mitotic catastrophe figures were less frequent than single vinorelbine. Karyolysis and karyorrhexis patterns became rarer. Occasional normal mitosis patterns were observed. Cisternal enlargement of ER membranes were less severe and less frequent than seen with single vinorelbine treatment. Autophagic changes were similar to vinorelbine group with lesser formation of gutta adipis. Cell cytoplasm
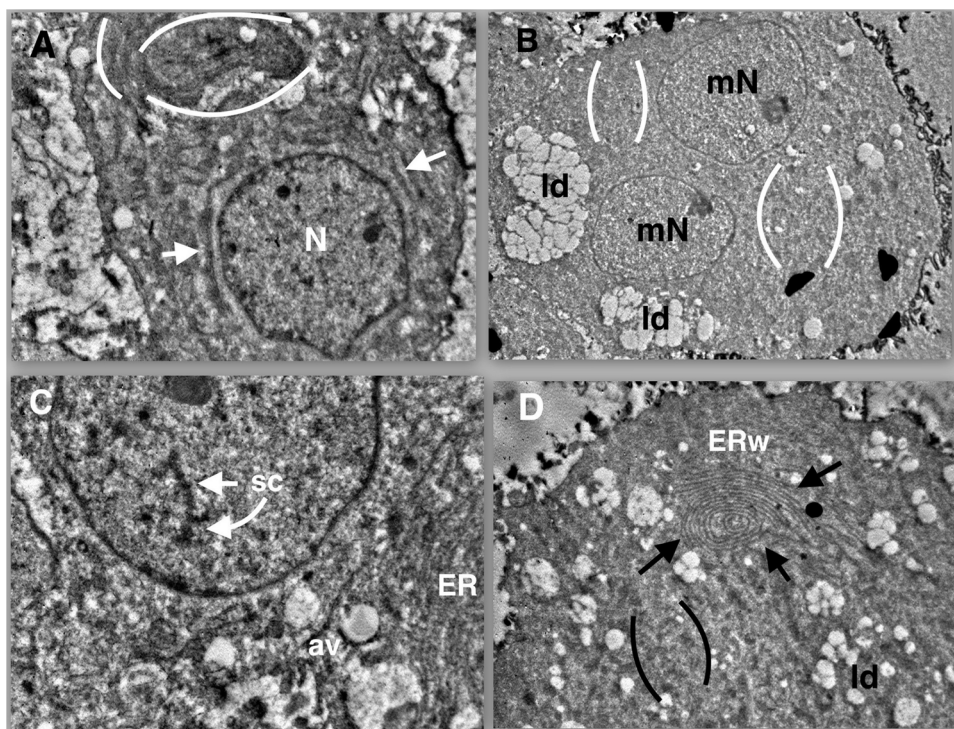


**Fig. 8.** Morphology of C6 glioblastoma cells in the gemcitabine + DMSO-treated group. Filopodia were lost. a) Endosomes with irregular electron luscent material exist in the cell periphery. Endoplasmic reticulum cisternae were enwidened (white curves) and occasionaly formed large stacks (surrounded by white curves) encasing some organelle material (x10000 m). b) Lipid droplet clusters in the cell periphery. Reduced number of condensed, darkened mitochondria (surrounded by white curves) which were difficult to discern within the cytoplasm (x 5000 m). Enwidened cisternae of endoplasmic reticulum (ER) and autophagic vacuoles (av) c) Synaptonemal complex (sc) within a cell nucleus (x 12000 m). d) Endoplasmic reticulum whorls (ERw), which did not surround other organelles rather collapsed within themselves (surrounded with black arrows). The cytoplasm contained shrunken mitochondria (surrounded with black curves) and abundant lipid droplets/gutta adipis (ld) (x 7500 m). m: magnification.
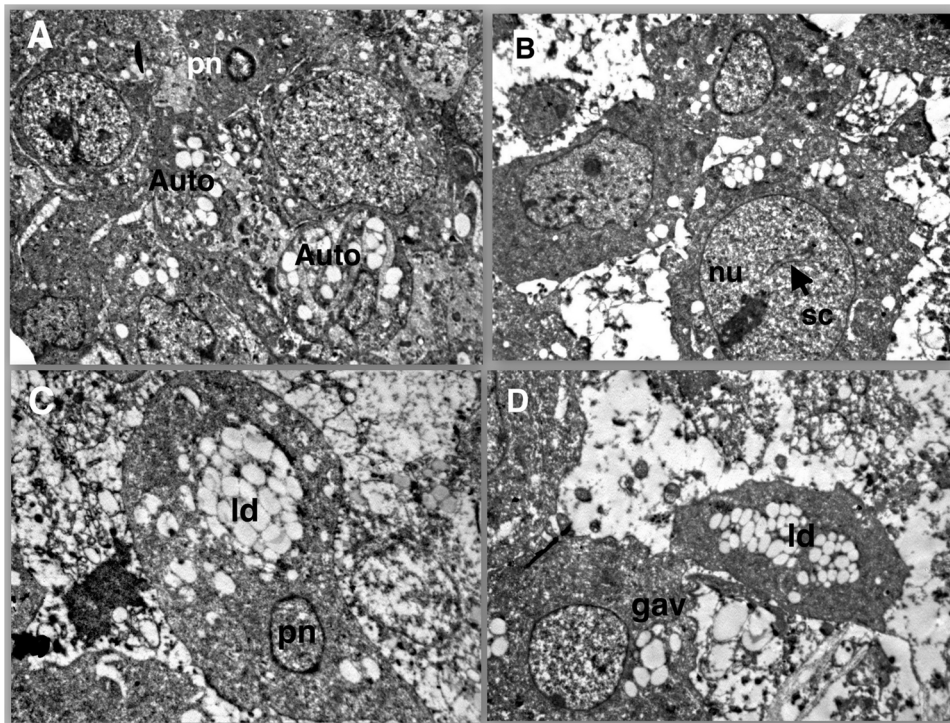
**Fig. 9.** Morphology of C6 glioblastoma cells in the gemcitabine + rofecoxib-treated group. Filopodia were lost. In general, autophagolysosomes enhanced further than the single gemcitabine-treated group and coalesced into clusters. a) Cells with pycnotic nuclei (pn) or complete autophagy (Auto) (x 5000 m). b) A large dense nucleolus (nu) and synaptonemal complex (sc) within a tumor cell nucleus (x 6000 m). c) Lipid droplets (ld) and pycnotic nucleus (pn) (x 5000 m). d) Cluster of lipid droplets (ld) and giant autophagic vacuoles (x 5000 m). m: magnification.

had lesser organelles. In some cells, ER cisternae surrounded mitochondria.

### 3.1.10. Vinorelbine + DMSO

Findings were quite similar to the Vinorelbine + rofecoxib combination (data not shown).

### 3.2. Plating efficacy in monolayer growth: dose response studies and drug combinations

Dose dependent effects of rofecoxib, gemcitabine and vinorelbine on monolayer growth of C6 glioblastoma cells were shown in Fig. 14. Fig. 15 depicts combined effects of same agents on monolayer growth of C6 glioblastoma cells. Vinorelbine reduced the cell numbers at all time points in comparison to control (p > 0.05 for the 24th hour, p < 0.01 for the 48th, 72th and 96th hours, respectively). There was no difference between 1 and 10 μg/ml (0.927 and 9.27 μM) in eliciting
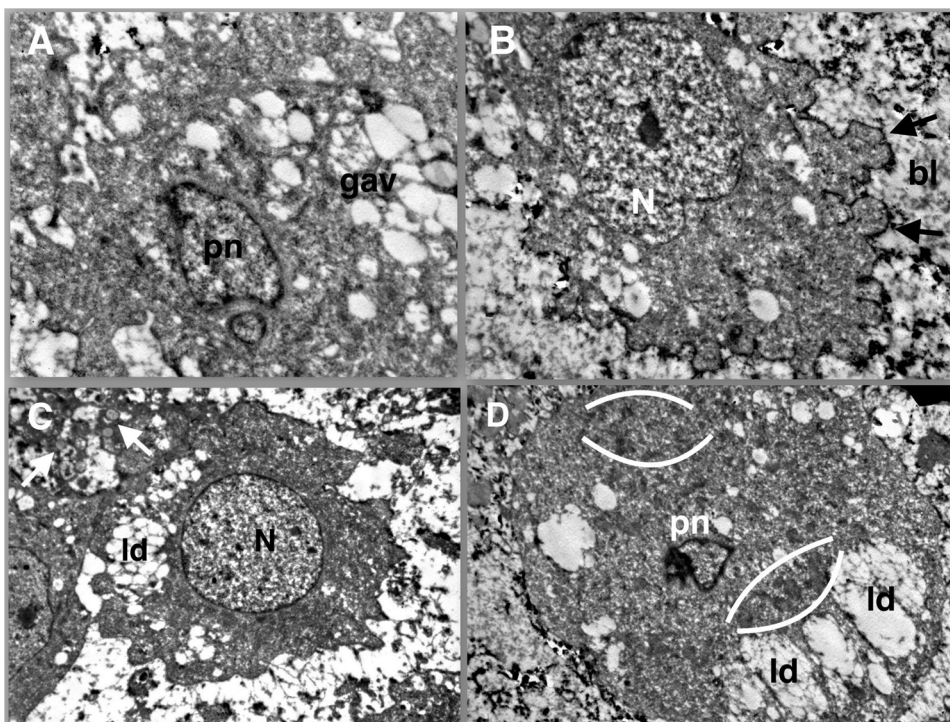


**Fig. 10.** Morphology of C6 glioblastoma cells in the gemcitabine + rofecoxib-treated group. a) A pycnotic nucleus. Juxtaposing giant autophagosomes (gav) (x 7500 m). b) Blebbing (bl) of the cytoplasmic membrane (black arrows) (x 7500 m). c) Autophagic vacuoles (x 5000 m). d) Lipid droplets (ld) juxtaposing dark condensed mitochondria (surrounded by white curves) (x 5000 m). m: magnification. Figure 2b was taken from the publication of Tuna et al. (2009) with permission (corresponding to the Figure 4c in the aforementioned manuscript).
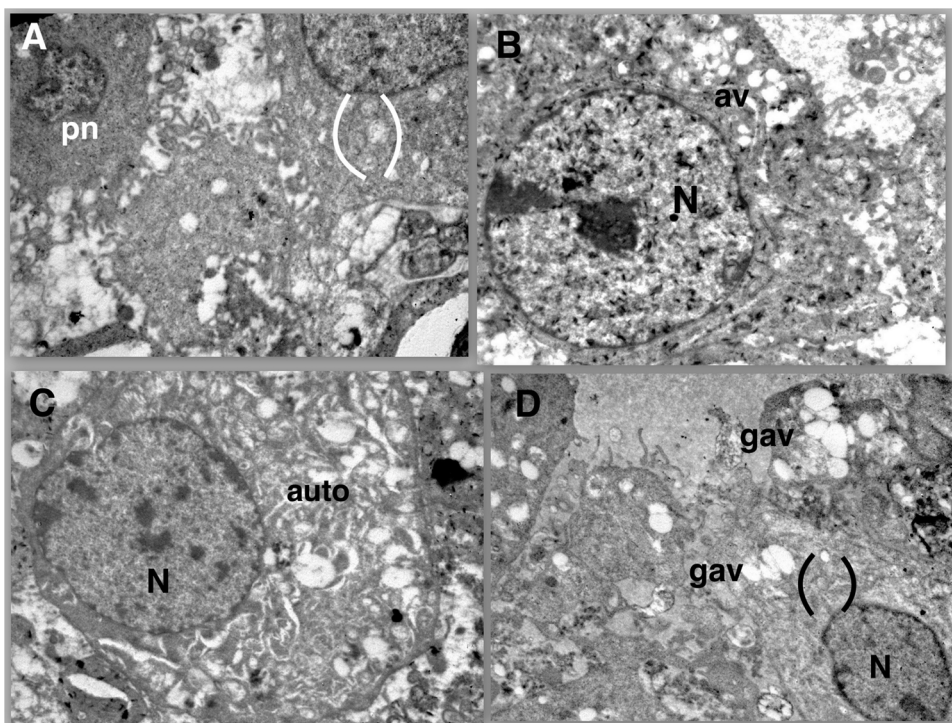
**Fig. 11.** Morphology of C6 glioblastoma cells in the vinorelbine-treated group. a) A pycnotic nucleus (pn). Mitochondria with crista damage (surrounded by white curves). b) Autophagic vacuoles (av) at the cell periphery (x10000 m). c) Autophagic vacuolization (auto) and cisternal enlargement of endoplasmic reticulum was so intense that cytoplasm was almost fragmented (x6000 m). d) Condensed mitochondria (between black arrows) were barely discernible. Giant autophagic vacuoles (gav) (x7500 m).

proliferation-inhibition (p > 0.05). Further, the activities of 1 and 10 μg/ml doses of vinorelbine to suppress cell growth did not increase further at the 72th and 96th hours (p > 0.05). On the other hand, vinorelbine at 100 μg/ml (92.7 μM) suppressed cell growth more potent than 1 and 10 μg/ml at the 48th hour (p < 0.05) with a progressive decline at the 72th and 96th hour. At the 96th hour, there were almost no surviving cells among cells treated with vinorelbine at 100 μg/ml (p < 0.01 in comparison to 1 and 10 μg/ml and p < 0.0001 in comparison to control, respectively). Gemcitabine was capable to reduce plating efficacy at the earliest time point (24 h), which slightly

decreased at the 48th hour, yet became progressively effective thereafter (72 and 96 h). There was no difference between 1–100 μg/ml (3.78–378 μM) of gemcitabine in reducing monolayer cell growth (p < 0.05 at all time points). Rofecoxib insignificantly reduced cell numbers in comparison to control and until the 72th hour and there was no difference between its different doses (3.18–318 μM) to alleviate growth. Furthermore, the slight growth-inhibitory effects of rofecoxib decreased at the 96th hour. DMSO reduced cell numbers by14,67% at the 24th hour, which was statistically significant (p > 0.05). But later, it did not reduce cell numbers (Fig. 15). The combination groups
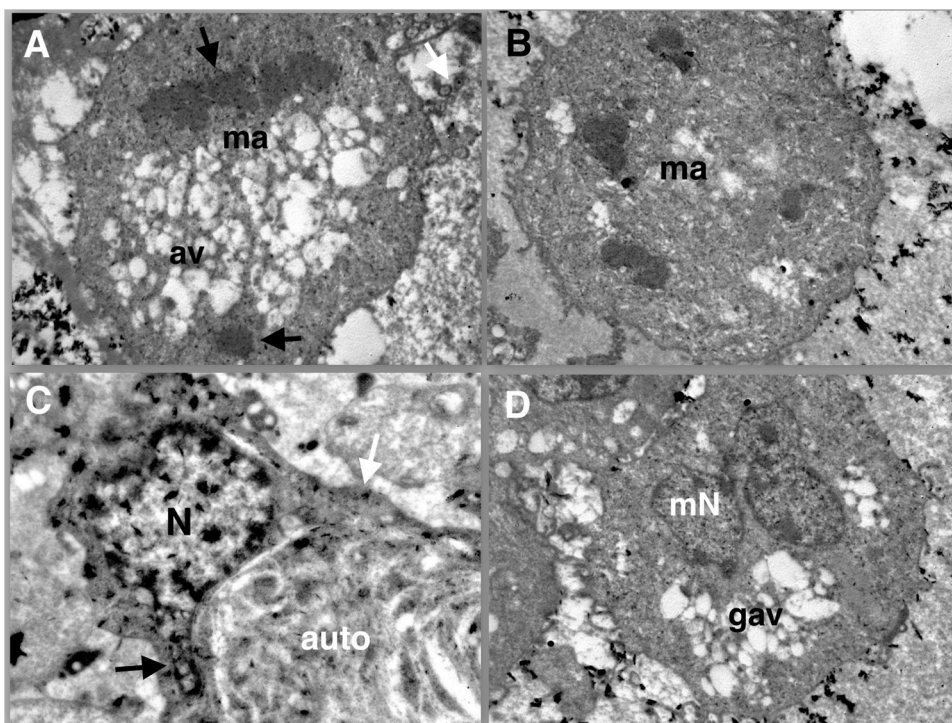


**Fig. 12.** Morphology of C6 glioblastoma cells in the vinorelbine-treated group. a) A mitotic apoptosis (ma) with accompanying prominent autophagy (av) (x75000 m). b) Another figure of mitotic apoptosis (ma) (x75000 m). c) A cell containing a nucleus with karyolysis and chromatin precipitation surrounds autophagic debris (auto) of a neighbouring cell (x15000 m). d) Karyorrhexis-multinuclei formation (mN) and prominent cytoplasmic autophagy (x7500 m).
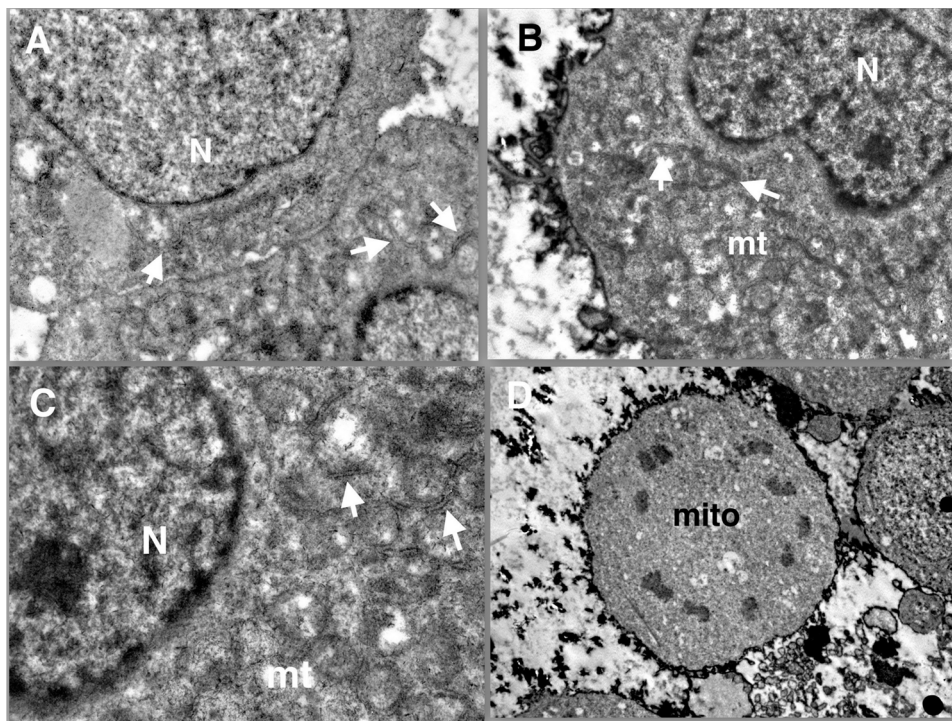
**Fig. 13.** Morphology of C6 glioblastoma cells in the vinorelbine + rofecoxib-treated group. In general, nuclear contours became similar to controls and indentations were seen less frequently. Mitotic catastrophe figures were less frequent than single vinorelbine. Karyolysis and karyorrhexis patterns became rarer. Cisternal enlargement of ER membranes much less frequent than seen with single vinorelbine treatment. Autophagic changes and formation of gutta adipis were much lower. a) A cell with normal nuclear (N) and cytoplasmic configuration and discernible membranes of endoplasmic reticulum (white arrows). b) Cell contained almost normal mitochondria (mt and white arrows). c) Mitochondria (m) were enwrapped with membranes of endoplasmic reticulum (white arrows). d) A tumor cell undergoing a fairly normal division (mito). Figure 13d was taken from the publication of Tuna et al. (2009) with permission (corresponding to the Figure 4d in the aforementioned manuscript).
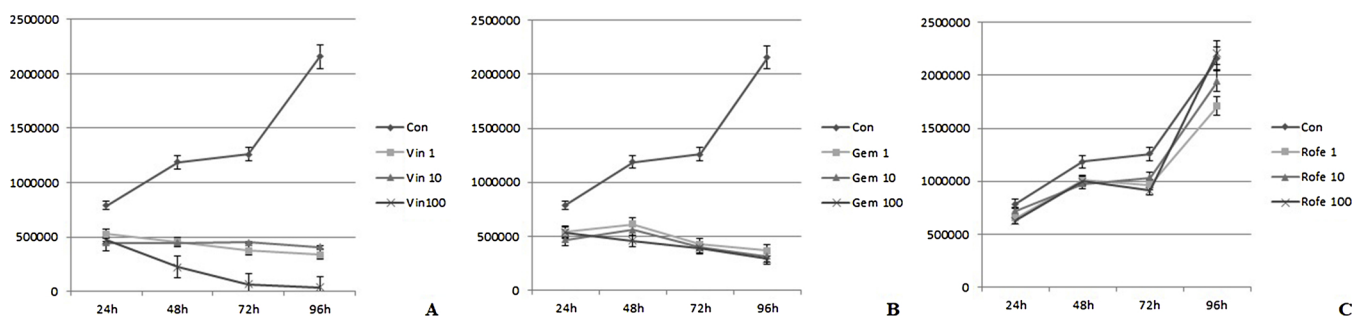


**Fig. 14.** Dose dependent effects of rofecoxib, gemcitabine and vinorelbine on monolayer growth of C6 glioblastoma cells. x axis represents time periods of cell counting and y axis represents cell numbers.

rofecoxib + vinorelbine and rofecoxib + DMSO significantly reduced the cell number in comparison to the control at all times ($p > 0.05$ for the 24th hour, $p < 0.01$ for the 48th, 72th and 96th hours, respectively). But these combinations were not superior to single vinorelbine treatment. The rofecoxib + gemcitabine combination also significantly reduced the cell number in comparison to the control at all times, but these reductions were also not superior to single gemcitabine treatment ($p > 0.05$ for all time points). When DMSO was combined with gemcitabine, growth inhibition reached to 85,51% at the 96th hour. This combination significantly reduced plating efficacies at all time points in comparison to control ($p < 0.05$, $p < 0.05$, $p < 0.01$ and $p < 0.01$ for 24, 48, 72 and 96th hours, respectively). But DMSO + gemcitabine combination was also not superior to single gemcitabine in reducing plating efficacy ($p > 0.05$ for all time points).

### 3.3. S-phase fraction as assessed with Brd-U labelling

Fig. 16 depicts the effects of DMSO (dimethylsulfoxide), rofecoxib (rofecox), vinorelbine (vin), gemcitabine (gem) and their combinations on the S-phase of C6 glioblastoma cell spheroid cultures. BrdU positive cells were observed both in the spheroid periphery and the centre of the controls. The labelling index of the control group was 18,2%. In the rofecoxib group, BrdU$^+$ cells were observed at the periphery of the spheroids and the BrdU-LI was determined as 8,5%, statistically lesser ($p < 0.01$) than the control group. The labelling index of the DMSO group was 9,1% and this was also significantly lesser in comparison to the control ($p < 0.01$). Gemcitabine drastically reduced the labelling of spheroids to 1,3%, which was significant in comparison to the control ($p < 0.01$). The labelling indices of the gemcitabine + rofecoxib and the gemcitabine + DMSO groups decreased to 1,5% and 1,6% which were significantly lesser than the control ($p < 0.01$ for both, respectively) but not different than the single gemcitabine ($p > 0.05$). Although vinorelbine decreased the BrdU-labelling of spheroids, this effect was heterogeneous because some spheroids exhibited high and some of them low labelling; yet the average labelling index following vinorelbine treatment was 7,3%, which was significantly lesser than control ($p < 0.01$). The average labelling of the vinorelbine + DMSO group was 10,6%, which was statistically significantly lesser than the control yet higher than the vinorelbine groups ($p < 0.05$ for both respectively). The average labelling of the vinorelbine + rofecoxib group was 14,8%, which was statistically significantly lesser than the control ($p < 0.01$) yet again higher than the single vinorelbine treatment ($p < 0.01$). Rofecoxib and DMSO significantly decreased the S-phase-inhibitory effect of vinorelbine.
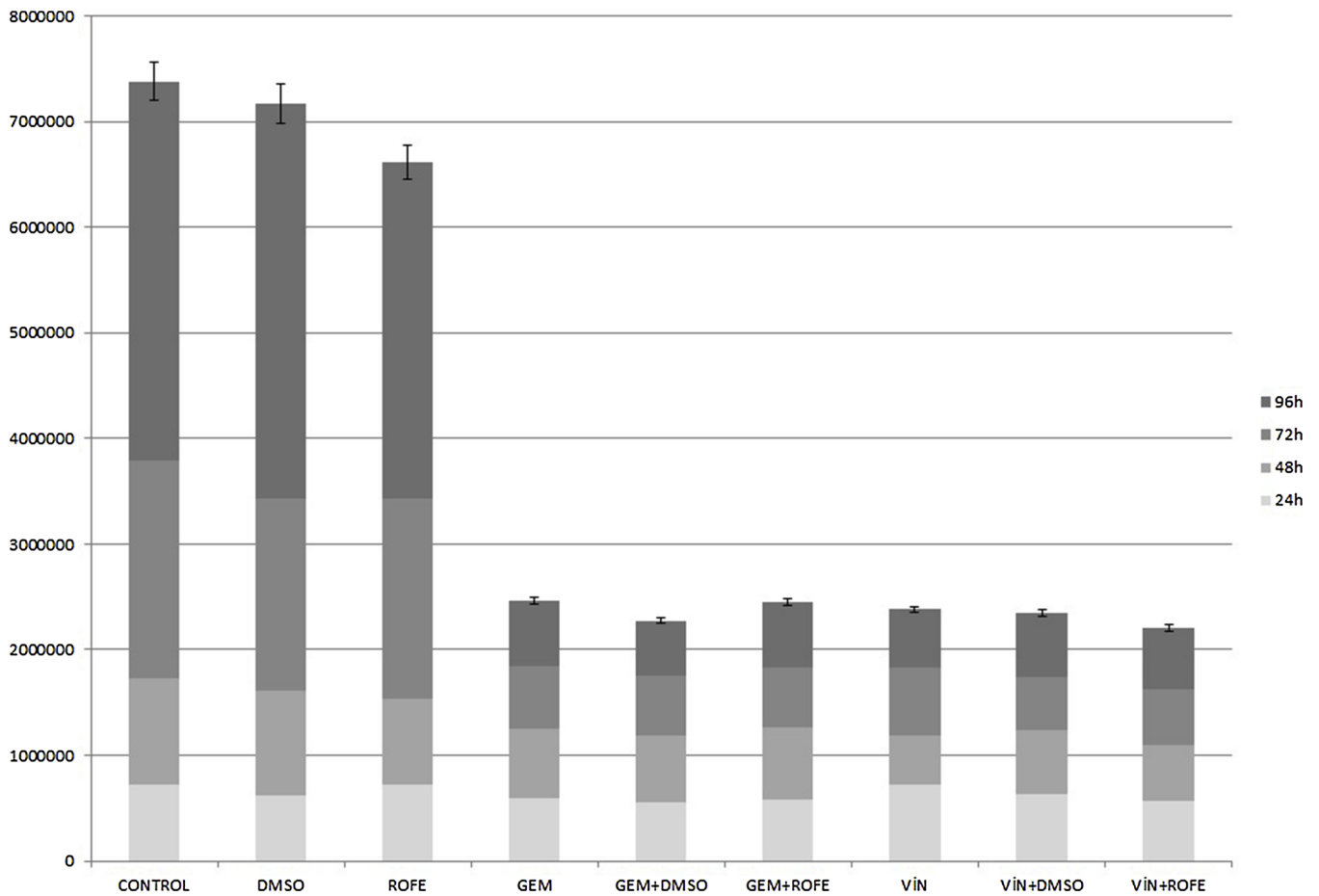
**Fig. 15.** Effects of DMSO (dimethylsulfoxide), rofecoxib (rofe), vinorelbine (vin), gemcitabine (gem) and their combinations on monolayer growth of C6 glioblastoma cells. x axis defines different drug applications and y axis represent cell counts. In each bar, different colours represent different time points which were explained at the right side of the figure with matching colours.
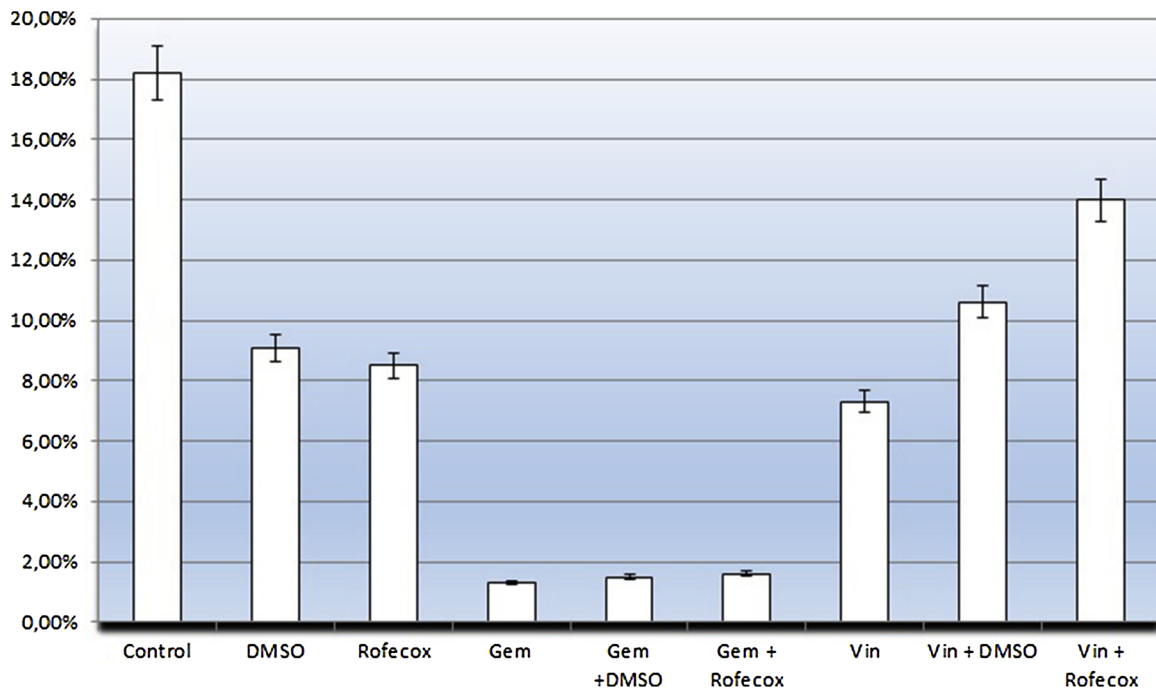


**Fig. 16.** Effects of DMSO (dimethylsulfoxide), rofecoxib (rofecox), vinorelbine (vin), gemcitabine (gem) and their combinations on the S-phase of C6 glioblastoma cell spheroid cultures. x axis represents different drug groups and y axis represents the percentage BrdU-labeling (suggesting the S-phase fraction) in spheroids following 72 hours after drug treatment (i.e. in the control group spheroids, 18,2% percent of cells were actively replicating their DNA, which reduced to 1,3% percent in gemcitabine-treated spheroids.).

## 4. Discussion

### 4.1. Potentials of vinorelbine, gemcitabine and cyclooxygenase inhibitors in glioblastoma

Vinorelbine arrests tumor cells in G2 and metaphase by blocking tubulin depolymerization and mitotic spindle formation (Hanley et al., 1998). Substitution of the catharanthine instead of the vindole moiety enhances lipophilicity, allowing enhanced diffusion of vinorelbine into cancer cells (Sato et al., 2007). First in 1998, vinorelbine was shown to block a number of human glioma cells inoculated into athymic nude mice (Hanley et al., 1998). Between 2008 and 2015, subsequent studies showed that vinorelbine may induce significant clinical responses in pontine and treatment-refractory progressive optic pathway gliomas, which have a fast and fatal course (Biassoni et al., 2006; Kuttesch et al., 2009; Massimino et al., 2008; Cappellano et al., 2011; Massimino et al., 2014; Cappellano et al., 2015). Gemcitabine (2′,2′-difluoro-2′-deoxy-cytidine) is a deoxycytidine analog and is an essential component of the chemotherapy protocols in a wide range of malignancies. The therapeuticity of gemcitabine starts with the intracellular triple phosphorylation by deoxycytidine kinase (dCK) to an active triphosphate form (dFdCTP) which competes with dCTP (deoxyCytidine Phosphate) for incorporation into DNA (Kudgus et al., 2013). 2016, it was reported that gemcitabine concurrent with radiotherapy was well-tolerated and yielded encouraging results in patients with high grade malignant glioma (Kim et al., 2016).

Increased COX-2 expression in human pancreatic cancers, as well as the growth-inhibitory effect of nonsteroidal anti-inflammatory drugs (NSAIDs) in vitro, led combinatory treatments of pancreatic cancer cells with gemcitabine and COX-inhibitors (Yip-Schneider et al., 2001). Phase-II clinical trials showed activity of gemcitabine, irinotecan and celecoxib in pancreatic cancer (Lipton et al., 2010). However, there exist no study which investigated whether gemcitabine efficacy could be augmented with COX-inhibitors in glioblastoma. Hence, we determined the actions of cyclooxygenase (COX) inhibitors alone and with chemotherapy on cell kinetics and ultrastructure of glioblastoma cells. As COX-inhibitors, we selected the non-selective cyclooxygenase inhibitor DMSO (dimethylsulphoxide) and COX-2 specific inhibitor rofecoxib. DMSO suppresses both prostaglandin formation and M2 subunit of ribonucleotide reductase (RR) (Bilir et al., 2004). The iron dependent RR enzyme catalyzes the formation of deoxyribonucleotides from nucleotides (Elledge et al., 1992) and it catalyzes a reaction that proceeds via a free radical mechanism of action (Eklund et al., 1997). Since gemcitabine also blocks M1 subunit of RR (Jordheim et al., 2011), we have anticipated a synergistic interaction with DMSO. Further, glioblastomas express higher levels of COX-2 and temozolomide treatment-potency is increased with celecoxib in orthotopic rat C6 glioblastoma model (Kang et al., 2006). Rofecoxib is withdrawn from the market due to its cardiovascular side effects (James et al., 2007); yet we employed it in this study due to its superselectivity on COX-2 (1000-times more inhibitory on COX-1 in comparison to COX-1) (Everts et al., 2000). Further, rofecoxib is a selective inhibitor of crinophagy, the disposal of excess secretory granules by lysosomes (Sandberg and Borg, 2006). To the best of our knowledge, our current study is the most detailed fine structural study, which investigated effects of gemcitabine, vinorelbine and cyclooxygenase inhibitors on glial tumor cells.

### 4.2. Are the selected in vitro dosages of vinorelbine and gemcitabine achievable in vivo?

Concentrations between 100 nM and 1 μM are peak plasma levels of vinorelbine in the conventional intravenous chemotherapy protocol (Biziota et al., 2016). But higher levels of vinorelbine may accumulate within tumor tissues due to its lipophilicity. Further, as will be also discussed below, Rabbani-Chadegani investigated effects of vinorelbine on normal bone marrow cells at concentrations similar to our cell culture conditions (10–160 μg/ml) (Rabbani-Chadegani et al., 2015). When they looked at PARP cleavage (a sign of apoptosis), they observed a dose-dependent increase; but a very faint band was seen at 10 μg/ml of vinorelbine. Hence, normal marrow cells are fairly tolerable to dosages around 10 μg/ml, which highly significantly suppressed proliferation of C6 glioblastoma cells. Our findings suggested that there was no difference between 1 to 100 μg/ml (3.78 to 378 μM) of gemcitabine in reducing monolayer cell growth. This may be explained with the fact that maximal inhibition of DNA synthesis and of many other metabolic pathways (which will be explained below) were already achieved at 1 μg/ml/3.78 μM. Indeed, some groups suggest that very low (IC50: 26 nM) dosages of gemcitabine block growth of pancreatic cancer, but other groups used dose ranges in pancreatic cancer cells, which were very similar to our dosages (Papademetrio et al., 2014). Apparaju et al. evaluated the gemcitabine concentrations in brain extracellular fluid (ECF) in normal rats and in ECF obtained from glioma-bearing rats (Apparaju et al., 2008). Studies on C6 glioma-bearing rats revealed that following an intravenous dose of 25 mg/kg, the AUC values in the tumor-free and tumor-brain regions were 4.52 ± 2.4, and 9.82 ± 3.3 μg h/ml, respectively (Apparaju et al., 2008). These results showed that we have applied achievable dosages and doses between 4 to 10 μM are proper to perform further experiments on gemcitabine in glioblastoma cells.

### 4.3. COX-inhibitor's effects on cell kinetics. Monolayer versus spheroid dichotomy

COX inhibitors did not influence monolayer growth of glioblastoma, but reduced S-phase in C6 glioblastoma spheroids. Here, it shall be noted that rofecoxib induced desmosomes between C6 glioma cells, indicating that antitumor efficacy of COX inhibitors may require 3-dimensional cell-to-cell contacts. In a bladder outlet obstruction model, which creates cellular stress on bladder epithelia, COX-2 inhibitors protect all types of cell-cell adhesions including zonula adherens, zonula occludens and gap junctions (Celik-Ozenci et al., 2006). Aspirin (a COX-1 and COX-2 inhibitor) is capable to augment expression of connexin-43, a component of gap junction in C6 glioblastoma cells (Qin et al., 2016). These data is compatible with our findings that COX-inhibitors did not modify monolayer growth yet blocked S-phase of spheroid cultures likely via enhanced cell-to-cell contacts.

### 4.4. DMSO induction of autophagy, mitochondrial changes and apoptosis

Dimethylsulphoxide (DMSO) was shown to both stabilise the lysosomal membranes and to trigger lysosomal activity (Misch and Misch, 1967). These differences may relate with its different different dosages and actions on different cells. In Paramecium cells, DMSO blocks cell proliferation at a concentration of 2% (same dosage that we have applied on C6 glioma cells) and above this concentration, it acted cytotoxic (Fok and Valin, 1983). In same cells, DMSO exerted a dose- and time-dependent inhibitory effect on the rate and size of digestive vesicle formation (Fok and Valin, 1983). Nonetheless, in Drosophila, DMSO acts as a chemical stressor to induce autophagy (Braden and Neufeld, 2016). DMSO effects on mitochondria are also dichotomous. A low dose of DMSO (0.1%) protects U937 lymphoma cells against 7β-hydroxycholesterol-induced cell death by preventing lysosomal and mitochondrial membrane permeabilization and reactive oxygen species (ROS) production (Laskar et al., 2010). On the other hand, a higher dose of DMSO (2.5%) could directly trigger mitochondria-driven apoptosis in EL-4 lymphoma cells via reducing bcl-2, collapse of mitochondrial membrane potential, and release of cytochrome C (Liu et al., 2001). In our study, DMSO (2%) triggered morphological hallmarks of apoptosis and autophagy, reduced the number and enhances the electron-density of mitochondria. Mitochondrial condensation, but not swelling is an earlier sign of apoptosis (Altinoz et al., 2007a), which was frequent amont DMSO-treated glioma cells.

### 4.5. Rofexocib induced mitochondrial injury, autophagy and lysosomal phospholipidosis. Still any role in future management of glioblastoma?

In our study, we revealed mitochondrial damage, ER stress, enhanced autophagy and myelinosis (whorl formations suggesting lysosomal phospholipidosis) in rofecoxib-exposed C6 glioblastoma spheroids. In adrenal tissues of rofecoxib treated rats, greater number of vacuoles and large lipid droplets containing cholesterol and other lipids were witnessed (Matysiak and Jodłowska-Jedrych, 2010). Prominent ER cisternae accompanied to large droplets and mitochondrial injury were also noticed. These findings are very similar to our results. Coxibs, such as rofecoxib, celecoxib, and valdecoxib raise levels of arachidonic acid, which then inhibit mitochondrial oxidative phosphorylation (OXPHOS) and increase ROS (Fosslien, 2005). But there exist also cellular injury mechanisms peculiar to rofecoxib (Mason et al., 2006). Experimental findings indicate that the cardiotoxic effects of rofecoxib may not be a class effect but because of its intrinsic chemical properties. Independently of COX-2 inhibition, rofecoxib increases oxidation of cellular membrane lipids, promotes the nonenzymatic formation of isoprostanes and reactive aldehydes (Mason et al., 2006). Cationic amphiphilic drugs such as tricyclic antidepressants are toxic to both cardiac and glioblastoma cells and induce significant myelinosis (Altinoz et al., 2007b). A relatively recent study showed that rofecoxib strongly sensitized glioblastoma stem cells to the oncolytic virotherapy by myxoma virus (McKenzie et al., 2015); which may be harnessed in future treatment strategies.

### 4.6. Synaptonemal complex formation in tumor cell nuclei. What could this mean?

Synaptonemal complex is a zipper-like intranuclear structure which forms between homologous chromosomes during meiosis mediating chromosome synapsis. Until now, they were only described in germ cells. It is well established that cancer cells regain stem cell phenotypes and could activate early embryonic genes. But could they express even genes of germ cells and form meiotic material? One of the cancer-testis antigens, which is expressed on cancer cells and testicular tissue is synaptonemal complex protein 1 (SCP-1) (Türeci et al., 1998); and strikingly, its frequent expression occurs is recently shown in malignant gliomas (Seo et al., 2016). We encountered these structures in treatment groups and it would be tempting to investigate whether antitumor drugs may trigger an aberrant meiotic process.

### 4.7. COX-inhibitors reduced vinorelbine-triggered mitotic slippage, but their combination induced mitotic slippage. How?

Mitotic slippage is the incapability of cells to remain in a mitotic arrested state for prolonged periods and replicating their DNA without cytokinesis causing enhanced aneuploidy and subsequent induction of a specific cell death described as "mitotic apoptosis" or "mitotic catastrophe". In our study, COX-inhibitors blocked vinorelbine-induced mitotic catastrophe, yet combination of DMSO with rofecoxib induced mitotic apoptosis. CUGBP2 (CUG triplet repeat-binding protein 2) is a ubiquitously expressed protein that interacts with CUG repeats and regulates versatile RNA pathways (Ramalingam et al., 2008). CUGBP2 induces the stability of COX-2 mRNA but it may also inhibit translation of COX-2 mRNA. CUGBP2 variant 1 causes cells to undergo mitotic catastrophe following radiotherapy (Ramalingam et al., 2008). Here, there might be a context-dependent difference between CUGBP2 induction and modification of COX-2. COX-2 activation may reduce mitotic apoptosis in response to various conditions (eg. microtubule poisons) but its combined blockage with COX-1 may trigger mitotic apoptosis.

### 4.8. COX-inhibitors do not influence gemcitabine effects on C6 glioblastoma cell kinetics

Since glioblastomas express higher levels of COX-2 and since temozolomide treatment-potency was shown to be increased with celecoxib in orthotopic rat C6 glioblastoma model (Kang et al., 2006), we also tried combinations with gemcitabine and inhibitors. We did not reveal any synergism with COX-inhibitors and gemcitabine neither in monolayer nor in spheroid S-phase indices. Nonetheless, since ultrastructural damage of tumor cells increased with combinations of gemcitabine and cyclooxygenase inhibitors, in vivo tumor responses may still be different.

### 4.9. Vinorelbine induction of mitotic apoptosis. Particular relevance for glioblastoma

Inhibition of microtubule dynamics by Vinca alkaloids involves in their efficacy to block mitosis. Vinorelbine treatment of human NSCLC PC-9 cells induced cell cycle arrest in the G2/M-phase, and when these cells were subsequently irradiated at a dose of 8 Gy, G2/M accumulation, hyperploidization and micronuclei formation occured (Fukuoka et al., 2001). Micro- and multinuclei formations are important signs of mitotic slippage/apoptosis induced by microtubule poisons (Nakayama and Inoue, 2016). Furthermore, post-slippage multinucleation induces further DNA damage and apoptosis and contributes to the cytotoxicity of microtubule inhibitors (Zhu et al., 2014). Nocodazole inhibits microtubule polymerization and induces arrest at mitosis and subsequently, it induces mitotic slippage of human U251 glioblastoma cells resulting in hyperploidization (Tsuiki et al., 2001). Glioblastoma cells seem to be particulary vulnerable to mitotic slippage/apoptosis. Okadaic acid (OA), a polyether fatty acid inhibits protein phosphatase 2A (PP2A) – responsible to repress the M-phase promoting factor – induces apoptosis of glioblastoma cells at very low concentrations below 5 nM (Castigli et al., 2006). Integrin linked kinase (ILK) provides organisation of centrosomal protein complexes; its blockage leads cancer cells to undergo multipolar anaphases and death in mitosis (Lanvin et al., 2013). Silencing ILK enhanced radiation-induced centrosome overduplication and mitotic apoptosis of glioma and overcame its intrinsic radioresistance (Lanvin et al., 2013). As mitotic death involves in radiotherapy efficacy, it would be plausible to test whether vinorelbine enhances efficacy of radiotherapy in glioblastoma.

### 4.10. Attenuation of vinorelbine-antineoplasticity with COX inhibitors. Inflammation may contribute to the tumoricidal activity of vinorelbine

We observed that COX-inhibitors significantly reduced vinorelbine efficacy to reduce the S-phase and to trigger mitotic apoptosis and autophagy. We think that these findings are concordant with unique effects of vinorelbine. Vinorelbine may induce an intense pain in cancer patients which is at the tumor site and unrelated to vinca neurotoxicity (Gebbia et al., 1994). Some authors suggested that patients with highly vascularized, oedematous and necrotic tumors are particularly vulnerable to this severe pain (De Marco et al., 1999). Enhanced COX activity and inflammation may positively contribute to the antitumor efficacy of vinorelbine. Vinorelbine's tumoricidal actions may also involve autophagy and ER stress. Application of autophagy inhibitors before vinorelbine treatment reduces its cytocidal activity, but their application subsequent to vinorelbine enhanced cell death of human lung cancer cells (Fu et al., 2008). In lung cancer cells, vinorelbine and SMAC (second mitocondrial activator of caspases)-mimetic exerted cytocidal synergism which involved enhanced ER-stress (Greer et al., 2011). Similarly, vinorelbine potentiates bortezomib-efficacy on myeloma cells accompanied by enhanced ER stress (Miyahara et al., 2016).

COX-inhibitors DMSO and rofecoxib induced mild autophagy alone, but reduced vinorelbine induced autophagy and ER stress. The reason behind this phenomenon may associate with the intensity of

prostaglandin synthesis. Skin cancer cells express enhanced levels of COX-2 which leads synthesis of J-series of prostaglandins (prostamides) at basal levels, yet if COX-2 activity is further increased, prostamides trigger ER-stress and cell death (Soliman et al., 2016). Edelfosine (ET-18-O-CH(3), a synthetic alkyl-lysophospolipid) induces apoptosis and COX-2 activation in ras-oncogene transfected breast cancer cells and COX-2 inhibitor celecoxib attenuated its apoptotic activity (Na and Surh, 2002). Hence, in certain conditions, COX-2 activation may contribute to antitumor efficacy of certain antineoplastic drugs and its inhibition may alleviate tumoricidal activity. In our study, rofecoxib was slightly more potent than DMSO to alleviate vinorelbine's antitumor efficacy. This may be due to rofecoxib's selective inhibition of crinophagy (Sandberg and Borg, 2006), the disposal of excess secretory granules by lysosomes. Cancer cells exposed to spindle poisons may require the material in the secretory granules to salvage cellular building blocks.

### 4.11. Gemcitabine treatment and changes in nuclear chromatin material

Prominent karyolysis of the central heterochromatin and margination of coarse chromatin towards the nuclear membrane was seen in gemcitabine-treated cells. Wrapping of nuclear histone proteins around DNA is important for resistance to gemcitabine, as histone deacetylase inhibitors sensitize cancer cells against gemcitabine (Fuino et al., 2003). Hence, transcriptional repression seems as an important protective response of tumor cells against gemcitabine, which is strongly supported by signs of endoplasmic stress (cisternal enlargement) and ER-whorl formation, which will be explained below. Gemcitabine also shortens telomeres (Su et al., 2012) and decreases the number of double minute chromosomes in cells at a 7500-times lower concentration than the chemotherapeutic hydroxyurea (Yu et al., 2013). Double minute chromosomes, including amplified oncogenes and drug-resistance genes, frequently exist in cancer cells and their elimination effectively decreases the malignancy of cancer (Yu et al., 2013).

### 4.12. Gemcitabine induction of autophagy. Friend or foe?

Abundant autophagy and gutta adipis (lipid droplet) formation prevailed in gemcitabine-treated C6 glioblastoma cells. In combinations of gemcitabine with DMSO or rofecoxib, these structures enhanced and coalesced into clusters. In 2013, Papademetrio et al. claimed that autophagy is responsible for the resistance of pancreatic tumors to gemcitabine (Papademetrio et al., 2014). Their selected dosages in vitro were high (0.001, 0.1, 1, 10, 100 μg/ml); and similar to our results on 72 h after treatment, there was not much difference between dosages of 0.01 to 10 μg/ml, but a significant rise of cell death occured when the dosage increased from 10 μg/ml to 100 μg/ml (Papademetrio et al., 2014). On the other hand, Fiorini et al. showed that Onconase® (ONC, a member of the RNase super-family that is secreted in oocytes) induced autophagy and sensitized pancreatic cancer cells to gemcitabine (Fiorini et al., 2015). In vivo studies are necessary, whether autophagy augmented with COX-inhibitors would increase tumoricidal activity of gemcitabine in glioblastoma.

### 4.13. Gemcitabine induction of mitochondrial changes and formation of gutta adipis/lipid droplets

In our study mitochondria were either shrunken or lost in gemcitabine and gemcitabine + COX inhibitor treated cells. Gemcitabine could directly block mtDNA synthesis by inhibiting mitochondrial DNA polymerase holoenzyme (DNA polymerase-γ) (Di Cresce et al., 2015). Triggering ROS-production is one of the major tumoricidal mechanisms of gemcitabine as pancreatic cancer cells with lower basal ROS-levels are more resistant to gemcitabine (Di Cresce et al., 2015). Gemcitabine-activation of acid sphingomyelinase also triggers insertion of proapoptotic bax protein into the mitochondrial membrane and strongly

induces death of glioma cells. All these data are compatible with our findings showing damage and reduction of mitochondria with gemcitabine treatment in C6 cells. We observed formation of lipid droplets / gutta adipis with gemcitabine, which was enhanced with COX-inhibitors. Lipid droplets are not stagnant depot sites, instead they are dynamic metabolic organelles and their accumulation is determined with metabolic state of cells (Kory et al., 2016).

Within the skeletal myocytes, lipid droplets act as fuel depots for mitochondrial fat oxidation and usually juxtapose mitochondria to allow fast transport (Stephens et al., 2011). With ageing, the numbers of lipid droplets increase yet their association with mitochondria are disrupted (Stephens et al., 2011). Gamma-linolenic acid (GLA) inhibits Walker 256 tumor growth in vivo and doubles the triacylglycerol and lipid droplet-content within the tumor cells (Colquhoun, 2002). Simultaneously, the surface density of mitochondrial cristae reduces, along with reductions in contact sites and matrix granules. Enhancement of lipid droplets were also defined in cancer cells exposed to biological antitumor agents or antitumor microRNA. In renal carcinoma cells, miR-494 expression markedly increased multilamellar bodies and lipid droplets and reduced cell viability accompanied by increased cleaved PARP and autophagic LC3B protein (Dutta et al., 2016). Besides autophagy, LC3B involves in the formation of lipid droplets; and its conjugated form LC3-II associates with the phosphatidylethanolamine of the lipid droplet-membrane (Dutta et al., 2016). Formation of lipid droplets accompanies mitochondrial changes including their shortening, fragmentation and becoming more electron-dense (Dutta et al., 2016), which are exactly parallel to our findings in gemcitabine-treated C6 cells. In cells exerting simultaneous enhancement of autophagy and lipid droplets, a recycling process may occur which involves concurrent lipid accumulation and utilization, as lipid droplet digestion occurs via autophagy (Zhao et al., 2014).

### 4.14. Gemcitabine-induced enlargement of ER cisternae and formation of ER whorls. Collapsed ER whorls with gemcitabine + DMSO treatment

In our study, ER whorls surrounded pyknotic nuclei in gemcitabine treated C6 glioma cells. In gemcitabine + DMSO co-treated groups, cisternal enlargement of ER membranes and formations of stacks were seen; while in some cells, ER membranes formed whorls which collapsed within themselves. ER is the major site of protein synthesis, folding and modification. Noxious events including oxidative stress and glucose deprivation can damage the ER which causes accumulation of disrupted and misfolded proteins in the ER lumen, which leads to ER stress. Studies in 14 pancreatic cancer cells revealed that various IRE1-inhibitors (inositol-requiring enzyme-1, which blocks ER-stress response) induced apoptosis and sensitized to gemcitabine (Chien et al., 2014).

ER whorls which collapse within themselves develop in several conditions: 1- Nutritional starvation, hormonal starvation and blockage of anabolic metabolism (Price et al., 1977; Taira et al., 1981; Walsh et al., 1982; Kubasik-Juraniec et al., 2009), cellular stress (Dabholkar and Carmichael, 1987; Garthwaite et al., 1992), 2- Inhibition of protein or cholesterol synthesis (Lum and Wright, 1995), 3- Disruption of ER transport and Golgi Systems causing accumulation of large lipid droplets (Sanguinetti et al., 1995; Zhou et al., 2011), 4- Carcinogenesis (De Nicola et al., 1978; Wessely et al., 1982; Muakkassah-Kelly et al., 1988; Morroni and Barbatelli, 2001); 5- Germ cell development (Gremigni and Nigro, 1983; Kallenbach, 1984). ER whorls occur in pancreatic cells during fasting and demonstrated as inactive RER lamellae. Fasting induces ER-whorls in Mosquito intestinal epithelia whereas feeding with blood and subsequent aminoacid supply causes robutst unwinding of ER. Loss of ER protein Yip1A, providing proper ER/golgi membrane networks, or decrease of alpha-COPI coatomer protein induced collapse of ER structures into whorls. Cancer cells may not prefer to synthesize new proteins under stress conditions; instead they shunt aminoacids into pathways to provide energetic fuel. Indeed, polyribosomal

profiling in pancreatic cancer cells showed that gemcitabine induced pan- suppression of translation (Palam et al., 2015). Prominent induction of ER-whorls in C6 cells with gemcitabine and gemcitabine + DMSO treatments strongly suggest that these agents induced shortage of essential cellular molecules.

## 5. Conclusions

Comprehensive ultrastructural analysis of cancer cell responses against antitumor treatments may provide a deeper view on the action mechanisms of antineoplastic drugs. A best approach would be combining old and new methods, in which gene expression data are interpreted in the context of electron microscopical ultrastructural findings. In our future studies, we will repeat these studies in human glioma cells and interpret these findings with simultaneously applied microarray data. Gemcitabine and vinorelbine induced both overlapping and distinct fine structural actions within C6 glioblastoma tumor cells and understanding these mechanisms may help to develop better combinatorial strategies not just for glioma treatment but also for other types of malignancies, where their clinical efficacies are proven.

## Conflict of interest

None to declare.

## Acknowledgements

## References

Altinoz, M.A., Elmaci, I., Ince, B., Ozpinar, A., Sav, A.M., 2016. Hemoglobins, Hemorphins, and 11p15.5 chromosomal region in cancer biology and immunity with special emphasis for brain tumors. J. Neurol. Surg. A. Cent. Eur. Neurosurg. 77, 247–257.

Tuna, S., Altinoz, M.A., Karasu, A., Canbolat, A., Bilir, A., 2009. Selective COX-2 inhibitor (Rofecoxib) inhibits vinorelbine cytotoxicity in C6 glioma cells in vitro. Open Pathol. J. 3, 22–29.

Hanley, M.L., Elion, G.B., Colvin, O.M., et al., 1998. Therapeutic efficacy of vinorelbine against pediatric and adult central nervous system tumors. Cancer Chemother. Pharmacol. 42, 479–482.

Sato, H., Fukumoto, K., Hada, S., et al., 2007. Enhancing effect of connexin 32 gene on vinorelbine-induced cytotoxicity in A549 lung adenocarcinoma cells. Cancer Chemother. Pharmacol. 60, 449–457.

Biassoni, V., Casanova, M., Spreafico, F., Gandola, L., Massimino, M., 2006. A case of relapsing glioblastoma multiforme responding to vinorelbine. J. Neurooncol. 80, 195–201.

Kuttesch Jr, J.F., Krailo, M.D., Madden, T., Johansen, M., Bleyer, A., 2009. Children's Oncology Group. Phase II evaluation of intravenous vinorelbine (Navelbine) in recurrent or refractory pediatric malignancies: a Children's Oncology Group study. Pediatr. Blood Cancer 53, 590–593.

Massimino, M., Spreafico, F., Biassoni, V., et al., 2008. Diffuse pontine gliomas in children: changing strategies, changing results? A mono-institutional 20-year experience. J. Neurooncol. 87, 355–361.

Cappellano, A.M., Bouffet, E., Cavalheiro, S., Seixas, M.T., da Silva, N.S., 2011. Diffuse intrinsic brainstem tumor in an infant: a case of therapeutic efficacy with vinorelbine. J. Pediatr. Hematol. Oncol. 33, 116–118.

Massimino, M., Biassoni, V., Miceli, R., et al., 2014. Results of nimotuzumab and vinorelbine, radiation and re-irradiation for diffuse pontine glioma in childhood. J. Neurooncol. 118, 305–312.

Cappellano, A.M., Petrilli, A.S., da Silva, N.S., et al., 2015. Single agent vinorelbine in pediatric patients with progressive optic pathway glioma. J. Neurooncol. 121, 405–412.

Kudgus, R.A., Szabolcs, A., Khan, J.A., et al., 2013. Inhibiting the growth of pancreatic adenocarcinoma in vitro and in vivo through targeted treatment with designer gold nanotherapeutics. PLoS One 8, e57522. https://doi.org/10.1371/journal.pone. 0057522.

Kim, M.M., Camelo-Piragua, S., Schipper, M., et al., 2016. Gemcitabine Plus Radiation Therapy for High-Grade Glioma: Long-Term Results of a Phase 1 Dose-Escalation Study. Int. J. Radiat. Oncol. Biol. Phys. 94, 305–311.

Yip-Schneider, M.T., Sweeney, C.J., Jung, S.H., Crowell, P.L., Marshall, M.S., 2001. Cell cycle effects of nonsteroidal anti-inflammatory drugs and enhanced growth inhibition in combination with gemcitabine in pancreatic carcinoma cells. J. Pharmacol. Exp. Ther. 298, 976–985.

Lipton, A., Campbell-Baird, C., Witters, L., Harvey, H., Ali, S., 2010. Phase II trial of gemcitabine, irinotecan, and celecoxib in patients with advanced pancreatic cancer.

J. Clin. Gastroenterol. 44, 286–288.

Bilir, A., Guneri, A.D., Altinoz, M.A., 2004. Acetaminophen and DMSO modulate growth and gemcitabine cytotoxicity in FM3A breast cancer cells in vitro. Neoplasma 51, 460–464.

Elledge, S.J., Zhou, Z., Allen, J.B., 1992. Ribonucleotide reductase: regulation, regulation, regulation. Trends Biochem. Sci. 17, 119–123.

Eklund, H., Eriksson, M., Uhlin, U., Nordlund, P., Logan, D., 1997. Ribonucleotide reductase–structural studies of a radical enzyme. Biol. Chem. 378, 821–825.

Jordheim, L.P., Sève, P., Trédan, O., Dumontet, C., 2011. The ribonucleotide reductase large subunit (RRM1) as a predictive factor in patients with cancer. Lancet Oncol. 12, 693–702.

Kang, S.G., Kim, J.S., Park, K., Kim, J.S., Groves, M.D., Nam, D.H., 2006. Combination celecoxib and temozolomide in C6 rat glioma orthotopic model. Oncol. Rep. 15, 7–13.

James, M.J., Cook-Johnson, R.J., Cleland, L.G., 2007. Selective COX-2 inhibitors, eicosanoid synthesis and clinical outcomes: a case study of system failure. Lipids 42, 779–785.

Everts, B., Währborg, P., Hedner, T., 2000. COX-2-Specific inhibitors–the emergence of a new class of analgesic and anti-inflammatory drugs. Clin. Rheumatol. 19, 331–343.

Sandberg, M., Borg, L.A., 2006. Intracellular degradation of insulin and crinophagy are maintained by nitric oxide and cyclo-oxygenase 2 activity in isolated pancreatic islets. Biol. Cell 98, 307–315.

Biziota, E., Briasoulis, E., Mavroeidis, L., Marselos, M., Harris, A.L., Pappas, P., 2016. Cellular and molecular effects of metronomic vinorelbine and 4-O-deacetylvinorelbine on human umbilical vein endothelial cells. Anticancer Drugs 27, 216–224.

Rabbani-Chadegani, A., Paydar, P., Amirshenava, M., Aramvash, A., 2015. An in vitro study on the effect of vinca alkaloid, vinorelbine, on chromatin histone, HMGB proteins and induction of apoptosis in mice non-adherent bone marrow cells. Drug Chem. Toxicol. 38, 220–226.

Papademetrio, D.L., Cavaliere, V., Simunovich, T., et al., 2014. Interplay between autophagy and apoptosis in pancreatic tumors in response to gemcitabine. Target Oncol. 9, 123–134.

Apparaju, S.K., Gudelsky, G.A., Desai, P.B., 2008. Pharmacokinetics of gemcitabine in tumor and non-tumor extracellular fluid of brain: an in vivo assessment in rats employing intracerebral microdialysis. Cancer Chemother. Pharmacol. 61, 223–229.

Celik-Ozenci, C., Ustunel, I., Erdogru, T., Seval, Y., et al., 2006. Ultrastructural and immunohistochemical analysis of rat uroepithelial cell junctions after partial bladder outlet obstruction and selective COX-2 inhibitor treatment. Acta Histochem. 107, 443–451.

Qin, L.J., Jia, Y.S., Zhang, Y.B., Wang, Y.H., 2016. Cyclooxygenase inhibitor induces the upregulation of connexin-43 expression in C6 glioma cells. Biomed. Rep. 4, 444–448.

Misch, D.W., Misch, M.S., 1967. Dimethyl sulfoxide: activation of lysosomes in vitro. Proc. Natl. Acad. Sci. U. S. A. 58, 2462–2467.

Fok, A.K., Valin, E.L., 1983. Effects of dimethylsulfoxide (DMSO) on the digestive-lysosomal system in Paramecium caudatum. Eur. J. Cell Biol. 32, 45–51.

Braden, C.R., Neufeld, T.P., 2016. Atg1-independent induction of autophagy by the Drosophila Ulk3 homolog. ADUK FEBS J 283, 3889–3897.

Laskar, A., Yuan, X.M., Li, W., 2010. Dimethyl sulfoxide prevents 7β-hydroxycholesterol-induced apoptosis by preserving lysosomes and mitochondria. J. Cardiovasc. Pharmacol. 56, 263–267.

Liu, J., Yoshikawa, H., Nakajima, Y., Tasaka, K., 2001. Involvement of mitochondrial permeability transition and caspase-9 activation in dimethyl sulfoxide-induced apoptosis of EL-4 lymphoma cells. Int. Immunopharmacol. 1, 63–74.

Altinoz, M.A., Bilir, A., Gedikoglu, G., Ozcan, E., Oktem, G., Muslumanoglu, M., 2007a. Medroxyprogesterone and tamoxifen augment anti-proliferative efficacy and reduce mitochondria-toxicity of epirubicin in FM3A tumor cells in vitro. Cell Biol. Int. 31, 473–481.

Matysiak, W., Jodłowska-Jedrych, B., 2010. Does administration of non-steroidal anti-inflammatory drug determine morphological changes in adrenal cortex: ultrastructural studies. Protoplasma 246, 109–118.

Fosslien, E., 2005. Cardiovascular complications of non-steroidal anti-inflammatory drugs. Ann. Clin. Lab. Sci. 35, 347–385.

Mason, R.P., Walter, M.F., McNulty, H.P., et al., 2006. Rofecoxib increases susceptibility of human LDL and membrane lipids to oxidative damage: a mechanism of cardiotoxicity. J. Cardiovasc. Pharmacol. 47 (Suppl 1), S7–14.

Altinoz, M.A., Gedikoglu, G., Sav, A., et al., 2007b. Medroxyprogesterone acetate induces c6 glioma chemosensitization via antidepressant-like lysosomal phospholipidosis/ myelinosis in vitro. Int. J. Neurosci. 117, 1465–1480.

McKenzie, B.A., Zemp, F.J., Pisklakova, A., et al., 2015. In vitro screen of a small molecule inhibitor drug library identifies multiple compounds that synergize with oncolytic myxoma virus against human brain tumor-initiating cells. Neuro Oncol 17, 1086–1094.

Türeci, O., Sahin, U., Zwick, C., Koslowski, M., Seitz, G., Pfreundschuh, M., 1998. Identification of a meiosis-specific protein as a member of the class of cancer/testis antigens. Proc. Natl. Acad. Sci. U. S. A 95, 5211–5216.

Seo, E.K., Choi, J.Y., Jeong, J.H., Kim, Y.G., Park, H.H., 2016. Crystal structure of C-Terminal coiled-Coil domain of SYCP1 reveals non-canonical anti-parallel dimeric structure of transverse filament at the synaptonemal complex. PLoS One(11), e0161379.

Ramalingam, S., Natarajan, G., Schafer, C., et al., 2008. Novel intestinal splice variants of RNA-binding protein CUGBP2: isoform-specific effects on mitotic catastrophe. Am. J. Physiol. Gastrointest. Liver Physiol. 294, G971–81.

Fukuoka, K., Arioka, H., Iwamoto, Y., et al., 2001. Mechanism of the radiosensitization induced by vinorelbine in human non-small cell lung cancer cells. Lung Cancer 34, 451–460.

Nakayama, Y., Inoue, T., 2016. Antiproliferative fate of the tetraploid formed after

Mitotic Slippage and its promotion; a novel target for Cancer therapy based on microtubule poisons. Molecules 21. https://doi.org/10.3390/molecules21050663. pii: E663.

Zhu, Y., Zhou, Y., Shi, J., 2014. Post-slippage multinucleation renders cytotoxic variation in anti-mitotic drugs that target the microtubules or mitotic spindle. Cell Cycle 13, 1756–1764.

Tsuiki, H., Nitta, M., Tada, M., Inagaki, M., Ushio, Y., Saya, H., 2001. Mechanism of hyperploid cell formation induced by microtubule inhibiting drug in glioma cell lines. Oncogene 20, 420–429.

Castigli, E., Sciaccaluga, M., Schiavoni, G., et al., 2006. GL15 and U251 glioblastoma-derived human cell lines are peculiarly susceptible to induction of mitotic death by very low concentrations of okadaic acid. Oncol. Rep. 15, 463–470.

Lanvin, O., Monferran, S., Delmas, C., Couderc, B., Toulas, C., Cohen-Jonathan-Moyal, E., 2013. Radiation-induced mitotic cell death and glioblastoma radioresistance: a new regulating pathway controlled by integrin-linked kinase, hypoxia-inducible factor 1 alpha and survivin in U87 cells. Eur. J. Cancer 49, 2884–2891.

Gebbia, V., Testa, A., Valenza, R., Cannata, G., Verderame, F., Gebbia, N., 1994. Acute pain syndrome at tumour site in neoplastic patients treated with vinorelbine: report of unusual toxicity. Eur. J. Cancer 30A, 889.

De Marco, S., Fabi, A., Ceribelli, A., Carlini, P., Pollera, C.F., Cognetti, F., 1999. Does pain at tumor site during vinorelbine infusion affect treatment of recurrent head and neck cancer patients? Ann. Oncol. 10, 865–866.

Fu, X., Pan, Y., Wang, J., Liu, Q., Yang, G., Li, J., 2008. [The role of autophagy in human lung cancer cell line A549 induced by Vinorelbine.]. Zhongguo Fei Ai Za Zhi. 11, 345–348.

Greer, R.M., Peyton, M., Larsen, J.E., et al., 2011. SMAC mimetic (JP1201) sensitizes non-small cell lung cancers to multiple chemotherapy agents in an IAP-dependent but TNF-α-independent manner. Cancer Res. 71, 7640–7648.

Miyahara, K., Kazama, H., Kokuba, H., et al., 2016. Targeting bortezomib-induced aggresome formation using vinorelbine enhances the cytotoxic effect along with ER stress loading in breast cancer cell lines. Int. J. Oncol. 49, 1848–1858.

Soliman, E., Henderson, K.L., Danell, A.S., Van Dross, R., 2016. Arachidonoyl-ethanolamide activates endoplasmic reticulum stress-apoptosis in tumorigenic keratinocytes: role of cyclooxygenase-2 and novel J-series prostamides. Mol. Carcinog. 55, 117–130.

Na, H.K., Surh, Y.J., 2002. Induction of cyclooxygenase-2 in Ras-transformed human mammary epithelial cells undergoing apoptosis. Ann. N. Y. Acad. Sci. 973, 153–160.

Fuino, L., Bali, P., Wittmann, S., et al., 2003. Histone deacetylase inhibitor LAQ824 down-regulates Her-2 and sensitizes human breast cancer cells to trastuzumab, taxotere, gemcitabine, and epothilone B. Mol. Cancer Ther. 2, 971–984.

Su, C.H., Chu, W.C., Lan, K.H., et al., 2012. Gemcitabine causes telomere attrition by stabilizing TRF2. Eur. J. Cancer 48, 3465–3474.

Yu, L., Zhao, Y., Quan, C., et al., 2013. Gemcitabine eliminates double minute chromosomes from human ovarian cancer cells. PLoS One 8, e71988. https://doi.org/10.1371/journal.pone.0071988.

Fiorini, C., Cordani, M., Gotte, G., Picone, D., Donadelli, M., 2015. Onconase induces autophagy sensitizing pancreatic cancer cells to gemcitabine and activates Akt/mTOR pathway in a ROS-dependent manner. Biochim. Biophys. Acta 1853, 549–560.

Di Cresce, C., Figueredo, R., Rytelewski, M., et al., 2015. siRNA knockdown of mitochondrial thymidine kinase 2 (TK2) sensitizes human tumor cells to gemcitabine. Oncotarget 6, 22397–22409.

Kory, N., Farese Jr., R.V., Walther, T.C., 2016. Targeting fat: mechanisms of protein localization to lipid droplets. Trends Cell Biol. 26, 535–546.

Stephens, N.A., Skipworth, R.J., Macdonald, A.J., Greig, C.A., Ross, J.A., Fearon, K.C., 2011. Intramyocellular lipid droplets increase with progression of cachexia in cancer patients. J. Cachexia Sarcopenia Muscle 2, 111–117.

Colquhoun, A., 2002. Gamma-linolenic acid alters the composition of mitochondrial membrane subfractions, decreases outer mitochondrial membrane binding of hexokinase and alters carnitine palmitoyltransferase I properties in the Walker 256 rat tumour. Biochim. Biophys. Acta 1583, 74–84.

Dutta, P., Haller, E., Sharp, A., Nanjundan, M., 2016. MIR494 reduces renal cancer cell survival coinciding with increased lipid droplets and mitochondrial changes. BMC Cancer 16, 33. https://doi.org/10.1186/s12885-016-2053-3.

Zhao, L., Dai, J., Wu, Q., 2014. Autophagy-like processes are involved in lipid droplet degradation in Auxenochlorella protothecoides during the heterotrophy-autotrophy transition. Front. Plant Sci. 5, 400. https://doi.org/10.3389/fpls.2014.00400.

Chien, W., Ding, L.W., Sun, Q.Y., et al., 2014. Selective inhibition of unfolded protein response induces apoptosis in pancreatic cancer cells. Oncotarget 5, 4881–4894.

Price, M.T., Olney, J.W., Cicero, T.J., 1977. Proliferation of lamellar whorls in arcuate neurons of the hypothalamus of male rats treated with estradiol benzoate or cyproterone acetate. Cell Tissue Res. 182, 537–540.

Taira, K., Mutoh, H., Shibasaki, S., 1981. Freeze-fracture study on the whorls of rough endoplasmic reticulum in the exocrine pancreatic cells of the Japanese newt and African clawed toad. Cell Tissue Res. 220, 669–672.

Walsh, R.J., Brawer, J.R., Naftolin, F., 1982. Early postnatal development of the arcuate nucleus in normal and sexually reversed male and female rats. J. Anat. 135, 733–744.

Kubasik-Juraniec, J., Zauszkiewicz-Pawlak, A., Kotlarz, G., Woźniak, M., Knap, N., 2009. Ultrastructural response of arcuate nucleus neurons to fasting in aged rats. Folia Morphol (Warsz) 68, 218–223.

Dabholkar, A.S., Carmichael, W.W., 1987. Ultrastructural changes in the mouse liver induced by hepatotoxin from the freshwater cyanobacterium Microcystis aeruginosa strain 7820. Toxicon 25, 285–292.

Garthwaite, G., Hajos, F., Garthwaite, J., 1992. Morphological response of endoplasmic reticulum in cerebellar Purkinje cells to calcium deprivation. Neuroscience 48, 681–688.

Lum, P.Y., Wright, R., 1995. Degradation of HMG-CoA reductase-induced membranes in the fission yeast, Schizosaccharomyces pombe. J. Cell Biol. 131, 81–94.

Sanguinetti, R.E., Ogawa, K., Kurohmaru, M., Hayashi, Y., 1995. Ultrastructural changes in mouse Leydig cells after streptozotocin administration. Exp. Anim. 44, 71–73.

Zhou, G., Isoe, J., Day, W.A., Miesfeld, R.L., 2011. Alpha-COPI coatomer protein is required for rough endoplasmic reticulum whorl formation in mosquito midgut epithelial cells. PLoS One 6, e18150. https://doi.org/10.1371/journal.pone.0018150.

De Nicola, A.F., von Lawzewitsch, I., Kaplan, S.E., Libertun, C., 1978. Biochemical and ultrastructural studies on estrogen-induced pituitary tumors in F344 rats. J. Natl. Cancer Inst. 61, 753–763.

Wessely, Z., Shapiro, S.H., Scherer, J.D., 1982. Focal nodular hyperplasia of the liver: ultrastructural observations. Ann. Clin. Lab. Sci. 12, 119–125.

Muakkassah-Kelly, S.F., Bieri, F., Waechter, F., Bentley, P., Stäubli, W., 1988. The use of primary cultures of adult rat hepatocytes to study induction of enzymes and DNA synthesis: effect of nafenopin and electroporation. Experientia 44, 823–827.

Morroni, M., Barbatelli, G., 2001. Stages of development of the ribosome-lamella complex: an ultrastructural study. Ultrastruct. Pathol. 225, 335–343.

Gremigni, V., Nigro, M., 1983. An ultrastructural study of oogenesis in a marine triclad. Tissue Cell 15, 405–415.

Kallenbach, R.J., 1984. Endoplasmic reticulum whorls as a source of membranes for early cytaster formation in parthenogenetically stimulated sea urchin eggs. Cell Tissue Res. 236, 237–244.

Palam, L.R., Gore, J., Craven, K.E., Wilson, J.L., Korc, M., 2015. Integrated stress response is critical for gemcitabine resistance in pancreatic ductal adenocarcinoma. Cell Death Dis. 6, e1913. https://doi.org/10.1038/cddis.2015.264.